(2)

OFFICE OF NAVAL RESEARCH

Grant N00014-90-J-1971

R&T Code 4131001 phy

Technical Report No. 2

High Resolution Infrared Spectroscopy of 2-Fluoroethanol in a Molecular Beam

by

Christopher L. Brummel, Steven W. Mork, and Laura A. Philips

Prepared for Publication
in the
Journal of Chemical Physics

Cornell University
Department of Chemistry
Ithaca, NY 14853-1301

May 29, 1991

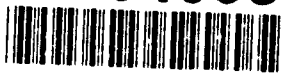

HIGH RESOLUTION INFRARED SPECTROSCOPY OF 2-FLUOROETHANOL IN A MOLECULAR BEAM

Christopher L. Brummel, Steven W. Mork, Laura A. Philips
Department of Chemistry, Cornell University, Ithaca, New York 14853

ABSTRACT

The high resolution infrared spectrum of 2-fluoroethanol (2FE) in a molecular beam was obtained in the region of 2990-2977 cm^{-1}. This spectral region contains the asymmetric CH stretch of the fluorinated carbon. Excitation of the CH stretch has previously been observed to photochemically isomerize 2FE from the Gg' to the Tt conformation. The high resolution spectrum of this transition provides the information necessary to quantitatively evaluate the amount of vibrational mode-coupling between the asymmetric CH stretch and the torsional reactive coordinate. Minimal amounts of vibrational mode-coupling was observed in the spectrum which is consistent with the slow photoisomerization rate. The correlation of the amount of mode-coupling and the isomerization rate supports the conclusion that mode-selective vibrational coupling plays an important role in the photochemical dynamics. It is further suggested that the strong intramolecular attractive interactions limit the magnitude of the vibrational mode-coupling.

INTRODUCTION

The present study uses high resolution spectroscopy in a molecular beam to explore both structure and dynamics in the isomerization of 2-fluoroethanol(2FE). The conformation of 2FE has been the subject of extensive study both experimentally and theoretically.[1-32] The most stable conformation of 2FE has been determined to be a slight distortion from the Gg' configuration, where the G refers to gauche orientation about the C-C bond and the g' refers to gauche orientation about the C-O bond. Microwave experiments have shown that this configuration has the O-H and C-F bond nearly antiparallel (+/- 5 degrees), with a CCOH dihedral angle of 55.5 degrees and an FCCO dihedral angle of 62.2 degrees.[2] The relative energy as a function of the C-C torsional angle is shown in a schematic diagram of the

potential curve for 2FE in Figure 1. The exceptional stability of the Gg' conformation makes 2FE particularly unusual, since one might expect steric interactions to favor the Tt (Trans-trans) conformation. The Tt conformation is the next most stable conformation, and has been experimentally determined to be over 900 cm^{-1} higher in energy than the Gg' in the gas phase.[3] This energy difference has been calculated to be anywhere from 224 cm^{-1} (STO-3G) to 819 cm^{-1} (MP3/6-31G*).[4,5] The barrier to rotation between Gg' and Tt has been determined to be 1600-1700 cm^{-1}, both theoretically and experimentally in low temperature matricies.[6,7] Although the Gg' conformation is also preferred in other 2-haloethanols, the energy difference is much less dramatic.[3,8] The strong stabilization of the Gg' conformer of 2FE has been attributed to a number of intramolecular interactions. The most popular explanation is hydrogen-bonding between the fluorine atom and the hydroxyl proton.[3,7,9,19-24] The C-F bond and the O-H bond, however, are nearly parallel making a classical hydrogen bond between the OH and F nearly impossible. Moreover, microwave and electron diffraction results have shown that the fluorine and hydrogen are roughly van der Waals distances apart[2,3,10] and that the electron distribution between the oxygen and hydrogen has cylindrical symmetry about the internuclear bond, indicating the unlikelihood of hydrogen bonding.[2,11] Other suggestions for stabilizing interactions include dipole-dipole attraction between the nearly antiparallel dipoles of the O-H and C-F bonds[10] as well as the "gauche effect"[3,12] and three atom "super-exchange" interactions involving the electrons on the fluorine, hydroxy proton and oxygen[11]. These intramolecular attractive interactions, while not completely understood for 2FE, clearly dictate the molecular conformation by affecting the overall molecular potential surface.

In addition to being structurally intriguing, 2FE exhibits interesting dynamics as well. A variety of different studies have probed the photoisomerization of 2FE between Gg' and Tt conformers while trapped in low temperature matrices.[1,6-8,12-18] By exciting either the OH or CH stretch in the matrix isolated molecule it is possible to induce an isomerization from the Gg' to the Tt conformer. The rate of the Gg'-to-Tt isomerization has been measured to be roughly 5 times faster than the reverse reaction.[17] In one study, the mechanism of the reaction was suggested to involve the surrounding matrix, requiring that the molecule be oriented so as to have a "favorable physical environment" with respect to the matrix.[13] The same study found that rates for isomerization depended not only on the matrix temperature, but also on the type of matrix site, suggesting matrix involvement in the mechanism. In contrast, other studies suggest that the isomerization is independent of the matrix.[6,14,16,18] If the mechanism is matrix independent, then the isomerization must result from intramolecular energy flow from the excited OH and CH stretches into the reactive coordinate, presumably involving a substantial amount of torsional motion about the C-C bond. Intramolecular energy flow requires that these different vibrational modes be coupled to facilitate efficient intramolecular energy transfer prior to cooling via collisions with the matrix. The relative quantum efficiencies for Gg'-to-Tt isomerization within an Ar matrix show that excitation of the OH stretch is approximately 7 times more efficient in inducing isomerization than the CH stretches.[16] Such mode-selective reaction rates suggest that the CH and OH stretches couple differently into the reactive coordinate. An investigation into the photoisomerization using polarized light found that the isomerization does not occur via a random increase in rotational energy, as one might expect if the matrix were to play a

significant role. Instead, isomerization involves only the rotation of the -CH_2OH end of the molecule with respect to the matrix.[14] This finding also supports the mode coupling model. By placing 2FE in a molecular beam, in the present study, the ambiguity of the environmental effects have been removed so that the presence of mode-coupling can be definitively determined.

Rotationally resolved spectra in molecular beams have been used to determine the geometrical structure of a variety of isolated molecules and complexes.[33-53] In addition to structural information, high resolution spectroscopy can provide direct evidence of the dynamics of vibrational energy flow within a single molecule.[33-39] For example, pyrazine has been the focus of many such studies due to its intermediate level of coupling between electronically excited zero-order singlet states and the lower triplet and ground singlet states.[33] While electronic spectroscopy has been extremely informative in the study of molecular potential surfaces, rotationally resolved vibrational spectroscopy has some additional advantages. For example, not all molecules of interest have an electronic chromophore which absorbs in spectral regions easily accessible by currently available laser technology. More importantly, electronic spectroscopy probes properties of the electronically excited state rather than the ground state. Questions concerning ground state structure and dynamics are, therefore, not addressed. In particular, experiments that use high resolution electronic spectroscopy to explore vibrational mode-coupling are plagued by the high density of states from the ground state continuum as well as lower electronic wells which are available to couple to the electronically excited state. Vibrational spectroscopy can explore the vibrational mode-coupling directly on the ground state potential surface where the density of states is more tractable. Consequently,

high resolution infrared spectroscopy is a valuable alternative for studying molecular conformation and dynamics in the ground state.

The power of high resolution infrared spectroscopy has been demonstrated in several previous studies. Conformational studies on isolated molecules and van der Waal's complexes have been studied using rotationally resolved vibrational spectroscopy.[34-48] High resolution infrared spectroscopy has additionally proven useful in studying intramolecular vibrational dynamics within the electronic ground state by resolving individual molecular eigenstates.[34-39] From the molecular eigenstates, vibrational mode coupling can be measured directly. de Souza, Kaun and Perry first used this technique to explore the molecular eigenstates in 1-butyne.[34,35] They found that their absorption spectrum of the acetylinic CH stretch of 1-butyne had more spectral transitions than expected. Their conclusion was that the $K_a'=0$ transitions are actually several transitions arising from coupling of the $K_a'=0$ zero-order states to a manifold of dark states with a density of about $100/cm^{-1}$. McIlroy and Nesbitt extended the study to a series of three terminal acetylenes (1-propyne[37], -butyne and -pentyne[38]) to compare coupling between zero order states. Their spectra clearly resolve the transitions to many molecular eigenstates within the acetylenic stretch of 1-butyne. In addition to the terminal acetylenes, Perry and coworkers have also measured the high resolution infrared spectrum of ethanol in a molecular beam.[36] Once again, mode-coupling was observed. If mode coupling occurs in 2FE, it should be evident in similar high resolution experiments. The extent of the coupling would be expected to correlate to the rate of the isomerization, if mode-selective coupling is responsible for the mechanism of isomerization. The present work explores the extent of

vibrational mode-coupling in the asymmetric CH stretch of the fluorinated carbon via the technique of high resolution infrared spectroscopy.

EXPERIMENTAL TECHNIQUE

The experimental apparatus consisted of three major components: 1) a high resolution scanning infrared laser system; 2) a molecular beam; and 3) a bolometer detection system. Each component is described in detail in the following sections. A diagram of the entire apparatus is shown in Figure 2.

Laser system:

The laser system included an argon ion pumped dye laser which pumped a Burleigh FCL-20 color center laser. Five watts of the 514 nm line from the argon ion laser (Coherent, Innova 15) was used to pump the kiton red dye laser (Coherent 599) which produced 1.3 W of red light. The wavelength of the dye laser was adjusted to maximize the power from the color-center laser. The equipment used to scan the frequency of the color-center laser at high resolution consisted of: a Macintosh II computer with a GWI MacADIOS A/D board; three ramp generators (Burleigh, RC-44, RC-43 and RC-46), two confocal etalons (Burleigh, FCL-975 free spectral range 7.5 GHz and CFT-100IR free spectral range 750 MHz); and a wavelength monitor (Digital Specialties).

The computer controlled the scanning of the color center laser. There were three adjustable elements in the color-center laser cavity which were monitored and adjusted during a scan: the end mirror, the intracavity etalon and the grating. To scan the laser the computer sent a voltage from 0-10V to the RC-44 ramp generator which amplified the voltage (~50 times) and sent it to the piezo stack that controlled the position of the laser end mirror. The RC-44 ramp generator also sent a voltages corresponding to 1/100 of the voltage

sent to the end mirror to the input of the RC-43 ramp generator. The RC-43 amplified the voltage (~25 times) and sent it to the piezo stacks that controlled the spacing of the intracavity etalon. The amount of amplification from the ramp generators depended on the particular scan. The gain on the RC-44 determined the frequency interval the laser covers in one scan. The gain on the RC-43 was set so that the etalon moved at such a rate that it stayed synchronous with the travel of the end mirror. These adjustments produced scans of approximately 0.12 cm^{-1}. After the computer completed a scan the end mirror and etalon were reset by sending a voltage of 0 V to the RC-44. The etalon was then scanned manually by increasing its bias voltage from the RC-43 until the laser had traveled approximately 0.11 cm^{-1}. A new scan was then begun which overlapped ~0.01 cm^{-1} with the previous scan. As scanning proceeded, the grating was adjusted manually as necessary.

Two confocal etalons monitored the frequency of the laser as it scanned. The 7.5 GHz etalon was used as a scanning etalon ramped by the RC-46 ramp generator at ~30 Hz. The output of the scanning etalon as well as the ramp voltage were sent to the Wavelength Monitor. The Wavelength Monitor digitized the position of the etalon transmission with respect to the voltage ramp and outputs a corresponding analogue voltage. The output voltage from the Wavelength monitor increased until a new transmission peak appeared. A new transmission appeared at the beginning of the ramp, at which time the output of the Wavelength Monitor dropped to zero. This procedure resulted in a sawtooth wave with a period equal to the free spectral range (7.5 GHz) of the scanning etalon. When the scan proceeded without any mode-hops in the laser, the sawtooth wave was smooth and continuous. Irregularities in the sawtooth wave were used to detect and correct for mode-hops during a scan.

The second etalon (750 MHz FSR) remained at a fixed separation. The output from this etalon was zero unless the laser was at a resonant frequency of the etalon. Thus, as the the laser was scanned a set of peaks was produced, each peak separated from the next by 750 MHz (the free spectral range of the etalon). These peaks were used to linearize the spectrum after the data was collected.

Data acquisition proceeded as the laser scanned. The computer stepped the laser one step (~1 MHz) and then read all the input channels 40 times, found the average for each channel and saved the data to a file. The data collected consisted of the output of the Wavelength Monitor, the signal from the fixed confocal etalon detector, the output of a power meter which monitors the laser power, and the signal from the bolometer detector.

Molecular Beam:

The molecular beam apparatus consisted of three differentially pumped vacuum chambers. The expansion chamber (Figure 2) was evacuated by an Edwards oil vapor booster pump (model 18B4) backed by a Kinney mechanical pump (model KT150). Pressure was monitored using an MKS Baratron capacitance manometer and was maintained at < 3 mtorr. The expansion chamber housed the molecular beam nozzle with a 50 μm diameter pinhole. The free jet is skimmed to form a molecular beam via a 1 mm skimmer located ~2.5 cm from the nozzle.

The molecular beam was crossed with the laser in the second chamber, the spectroscopy chamber. This chamber was pumped by a liquid nitrogen trapped 4" CVC blueline diffusion pump backed by a Leybold-Haraeus TRIVAC mechanical pump. The pressure of the spectroscopy chamber was monitored by an MKS ion-gauge with an MKS ion-gauge controller (type 290) and was maintained at 10^{-6} torr. The spectroscopy chamber contained a pair of parallel

mirrors located ~25 cm from the nozzle. These mirrors were used to repeatedly cross the focused laser beam with the molecular beam and were aligned such that the laser crossed the molecular beam in excess of 25 times. The mirrors were set parallel, with 1 cm separation, before placing them in the chamber, but the position of the pair of mirrors with respect to the molecular beam were adjusted from outside the vacuum chamber. The second chamber also housed a quadrupole mass-spectrometer (Inficon QX 2000) which was located perpendicular to the molecular beam and the laser. The mass spectrometer monitored the background gas in order assure that sample was in the molecular beam. The spectroscopy chamber connected to the bolometer chamber via a 10 mm aperture, which limited the influx of background gas into the bolometer chamber.

The bolometer chamber was pumped by a liquid nitrogen trapped Varian 6" diffusion pump which was backed by the same mechanical pump that backed the 4" blueline diffusion pump in the spectroscopy chamber. An MKS ion gauge controlled by a Inficon controller (IG3) was used to monitor the pressure, which was maintained at 10^{-7} torr. The bolometer chamber contained a liquid helium cooled bolometer (Infrared Laboratories Inc.) which was used as the detector for the experiment. In front of the detector was another aperture, 2 mm in diameter. The bolometer was located ~60 cm from the nozzle.

The sample was introduced into the molecular beam by flowing helium carrier gas through a cylindrical reservoir (~3 cm length, 1 cm dia) which contained glass wool saturated with the liquid 2-Fluoroethanol (~2 ml) at room temperature. The reservoir pressure of the helium carrier gas was 6.5 psig for most of the data collected.

Detection:

As described above after the molecular beam was skimmed it passed between two parallel mirrors where the laser beam intersected the molecular beam >25 times and then hit the bolometer. The bolometer consisted of a germanium doped silicon surface with a 2 mm by 6 mm diamond mounted on it to increase detector surface area. The rectangular surface of the diamond was oriented perpendicular to the path of the laser beam. The bolometer was cooled to ~1.6 K using liquid helium. To eliminate background noise, and enhance the sensitivity of the system, phase sensitive detection was used. The laser was chopped (~ 370 Hz) and the bolometer signal was monitored by a lock-in amplifier (Princeton Applied Research, model 5209). The phase of the lock-in amplifier was set to maximize the signal.

DATA

A spectrum of 2-fluoroethanol in a molecular beam was obtained in the region of 2990-2977 cm^{-1} using the high resolution infrared spectrometer described in the previous section. The vibrational transition that occurs in this region has previously been assigned to the asymmetric stretch of the hydrogens on the fluoronated carbon.[14]

The data were collected with two different experimental setups. In one configuration the laser beam intersected the molecular beam once. In the other configuration, the multipass device described above was used. Optimal resolution was obtained using the single pass configuration which resulted in a resolution of 7 MHz (FWHM), as show in Figure 3. The peak in Figure 3 was fit to both a Gaussian and a Lorentzian line shape. The Gaussian line shape gives a better fit suggesting that the line width is not lifetime limited but rather limited by laser frequency jitter and residual Doppler

broadening. When the multipass device was used the signal to noise ratio was increased by a factor of 8 while the resolution was reduced to 12 MHz FWHM. The small increase in the experimental line width resulted from increased Doppler broadening due the fact that the laser beam is no longer at ninety degrees with the molecular beam. The data presented, unless otherwise specified, was collected using the multipass configuration to enhance the signal-to-noise ratio.

Part of a typical scan is presented in Figure 4. A complete scan covers a spectral region of 0.1 cm^{-1}. The complete spectrum was assembled by concatenating approximately 100 individual scans to obtain the entire 10 cm^{-1} spectral region. Also shown in Figure 4 are the four traces obtained in each scan. Trace D is the lock-in amplified bolometer signal. Trace B is the output of a power meter, which monitored a fraction of the laser beam to determine laser power, and was used to normalize the data to fluctuations in the laser intensity. Intensities of the individual transitions must also be normalized to the desensitization of the bolometer with time. Bolometer desensitization was determined by scanning over a 2-fluoroethanol peak at 2982.99 cm^{-1} after every 5 scans. The intensity of this peak was used to determine the bolometer desensitization.

The remaining two traces in Figure 4 are signals from frequency monitoring devices used to determine the relative frequency during the scan. Trace C is the output of the scanning etalon after being processed by the Wavelength Monitor. As described above, the output from the Wavelength Monitor is a sawtooth wave. Trace A is the output of a fixed etalon, with a nominal free spectral range of 750 MHz. The etalon was calibrated at the beginning and end of each day. If the laser scanned linearly (in frequency) the marker peaks in trace A would be evenly spaced. Since the motion of the

piezo stacks which scan the laser were slightly nonlinear, the resulting laser scans were nonlinear in frequency. Thus, to obtain accurate relative frequencies a linear stretching or shrinking correction was applied to the spectrum so that the fixed etalon peaks are spaced at uniform intervals on the spectrum. These frequency markers were also useful in assembling the spectrum from individual scans.

The separate scans were collected such that the last marker peak (trace A) of a scan coincided with the first marker peak of the next scan. Since each frequency marker corresponded to a unique absolute frequency, all that was necessary to join two scans was to match up the last marker peak of the first scan with first marker peak of the second scan. This process was continued until the whole spectrum was assembled.

Once the spectrum was assembled the position and intensity of each peak was determined from the experimental data and stored in a two dimensional array. This method of data storage greatly facilitated data manipulations by reducing the number of data points the computers must manipulate from ~200,000 to ~1000 data points. Peaks were computer selected based on criteria that result in a minimum signal-to-noise ratio of 2. Once the computer selection was complete, the peaks were inspected manually to confirm that features selected were in fact peaks, and that no peaks were missed. The frequency of a peak was chosen to be that of the peak's maximum intensity. Since most of the peaks were very symmetric the frequency assignment should coincide with frequency assignments based on the centroid of the peak. After the peaks were selected their intensities were corrected for both bolometer desensitization and laser power as described above. The intensity correction was made after the peaks were selected. A bar graph rendition of the spectrum, where the x-coordinate is corrected peak frequency and the y-

coordinate is the corrected peak intensity, is displayed in Figure 5. The data contained in this bar graph spectrum is the experimental data that was used in the data analysis.

DATA ANALYSIS AND RESULTS

Once peaks were selected the next step was analysis of the data. The data was analyzed by an iterative procedure, whereby a simulated spectrum is calculated and compared to the experimental data. To calculate a spectrum it was necessary to determine ten parameters: the ground state and the excited state rotational constants, the projection of the transition moment onto the three inertial axes of the molecule, and the rotational temperature of the molecule in the molecular beam. A rigid rotor model was assumed and the spectrum was calculated based on an exact diagonalization of an asymmetric top rotational Hamiltonian.[54] The ground state rotational constants for 2-fluoroethanol were held constant at the values determined from previous microwave studies.[2] Reasonable guesses were assumed for the remaining parameters. The initial parameters were optimized with an iterative procedure based on a simplex search algorithm. The simplex optimization was repeated with many different starting parameters until the output spectrum began to resemble the experimental spectrum. Once the calculated spectrum began to resemble the experimental spectrum, it was possible to assign specific transitions in the spectrum (i.e. assign the quantum numbers of the ground and excited states for the transition). Because of the multitude of local minima in the chi squared parameter space, many simplex optimizations were necessary before quantum numbers could be assigned. With quantum numbers assigned for several of the transitions, the simplex optimization was much more efficient and the calculated fit to the data was refined. Improved

fits to the data were obtained with the use of two additional fitting routines: 1) a revised least squares optimization of the fit to the data, and 2) a combination differences analysis for both the ground and excited state rotational constants.[54]

It became evident that the experimental data had many more peaks than the calculated spectrum as the fitting proceeded. In particular, for many of the single peaks in the calculated spectrum there appeared to be several peaks in the experimental data. Obvious sources of extra peaks are: complexes formed in the molecular beam, other conformers, hot bands, and contaminants. These sources of extra peaks were all eliminated as follows. Complexes would have a negative bolometer signal as a result of predissociation of the complexes. Spectra of other conformers are known to be well separated from this frequency based on matrix work.[16] Hot bands would show a dramatic dependence on backing pressure, and again would not be expected in this spectral region. From an FTIR, an NMR and a mass spectrum of the liquid 2FE, no contaminant was evident. Since any contaminant would be present in extremely small quantities to escape detection by these analytical methods, any signal from a contaminant would be too small to be detectable in the molecular beam spectrum. Thus, we were able to eliminate these obvious sources of extraneous peaks.

The clusters of peaks are attributed to coupling between several different vibrational modes in the excited vibrational state. The rigid rotor model used to predict the rotational structure in the spectrum assumes that one vibrational mode carries all of the oscillator strength for the transition and is referred to as the light state. In addition to the light state there is a manifold of dark states--states that have little or no oscillator strength consisting of overtones and combinations of other vibrational modes. This basis set of light and dark states are eigenstates of a zeroeth order Hamiltonian that may be thought of as a first

approximation to the molecular eigenstates. Usually, for a molecule the size of 2FE the normal modes are used as the zeroeth order states. The light state is what has been identified qualitatively as the asymmetric stretch of the fluorinated carbon. If, instead, the true molecular eigenstates are a superposition of the light state with a number of dark states then one would expect the spectrum to become much more congested with peaks. The Hamiltonian for this coupled state picture would be the zeroeth order Hamiltonian plus a perturbation term which mixes the zeroeth order light and dark states. We observe in the spectrum of 2FE that the oscillator strength for each transition is distributed over a number of these mixed states resulting in clusters of peaks instead of single transitions. Figure 6a shows a diagrammatic representation of the light state and the manifold of dark states. In this figure, two transitions from different rotational states in the ground vibrational state to the same excited state are shown. In Figure 6b these states are mixed to form the true molecular eigenstates. When the excited state is mixed with the manifold of dark states, these single peaks become clusters of peaks as shown in Figure 6b. The two clusters of peaks exhibit the same pattern of intensities and frequencies, reflecting the same mixing in the excited vibrational state.

To confirm that mode-coupling is responsible for the clusters of peaks in the spectrum, we compared pairs of transitions to the same excited states. Figure 7 shows a representative sample of regions of the spectrum comparing such pairs of transitions. As shown in Figure 7, there is a clear similarity in the spacing and intensities of peaks in clusters that correspond to transitions to the same excited state. Clusters of peaks range from 2-5 peaks per cluster and span a spectral region of 0.0007-0.02 cm^{-1}. Quantum numbers were assigned to the cluster of peaks by using the same quantum numbers for all of the members of a particular cluster of peaks. No cluster of peaks was assigned without

matching the cluster to a second transition cluster to the same excited state. Combination differences were used to evaluate the accuracy of the assignment of quantum numbers. The RMS deviation in the energy level positions was determined to be 0.00066 cm^{-1} as calculated from 141 peaks in 40 different clusters. The small deviation confirms that the assignment of quantum numbers is correct. Table 1 contains all of the assigned peaks in the spectrum with their quantum numbers.

All of the assigned peaks presented in Table 1 correspond to C type transitions. No transitions resulting from a component of the transition moment along either the A or B axis could be identified. The criteria used to assign the spectrum were quite conservative. For example: 1) no clusters of peaks were assigned unless there were at least two transitions to the same excited state in the spectrum; 2) with few exceptions, clusters were not assigned that consisted of only 2 peaks, and those 2 peaks were required to have at least 3 transitions to the same excited state; and 3) no clusters of peaks were assigned that had insufficient signal-to-noise. As a result, there are many small peaks in the spectrum that were not identified that could conceivably be A or B type transitions. Therefore, we cannot be certain that the transition is completely C type. The dominant component of the transition moment, however, lies along the C axis.

To facilitate further refinement in fitting the data, these clusters of peaks were assimilated into a single peak for comparison with the calculated spectrum. The single peak corresponds to the frequency and intensity of the light state in the zeroeth order approximation. The frequency of the single peak was determined from a weighted average of the peaks in the clusters according to the method of Knight and coworkers.[55] In addition to determining the frequency and intensity of the light state, the method of

Knight and coworkers also evaluates the location of the dark states and the matrix elements that mix the light state with each of the dark states. Table 2 presents the location of the dark states with respect to the light states and the magnitude of the matrix elements.

This new spectrum, consisting of single peaks in place of the clusters of peaks, was used for the final stage of the analysis. As a check of the deconvolution procedure, the single peaks corresponding to transitions to the light states were used in a combination differences calculation. The RMS deviation of the energy level position from those predicted from the known ground state rotational constants is 0.00101 cm^{-1} from 40 combination differences. The larger error in these numbers are representative of an additional source of error that is introduced in the deconvolution procedure and caused by the measurement of spectral intensities. The errors in measuring the peak intensities is inherently much larger than the error in frequency determination. The intensity of a transition in a cluster of peaks, however, is indicative of the magnitude of mixing and therefore is required in the deconvolution procedure. To minimize the error in the determination of the excited state rotational constants, the ground state rotational constants were determined from the reduced data to be used in the least squares fitting procedure. The values of the ground state rotational constants determined here are compared to the microwave values in Table 3. The same source of error accounts for the discrepancy between the ground state rotational constants from the microwave experiments and our ground state rotational constants.

The ground state rotational constants determined from the reduced experimental spectrum were used to refine the excited state rotational constants using least squares optimization. The ground state rotational constants were held fixed while the excited state rotational constants and the frequency of the

0-0 transition were optimized by fitting calculated spectra to the experimental spectrum. All of the transitions used in the optimization were C type based on the assignment of individual transitions as discussed above. A source of error inherent in fitting the excited state rotational constants is the uncertainty in determining which peaks belong in a particular cluster of peaks. In some cases, there was ambiguity in assigning a peak to a cluster. Alternatively, some peaks may have been too small to identify and therefore were not included in the cluster. In either case, if a peak is missed, error is introduced in the deconvolution procedure. This error is reflected in the determination of the location of the transitions to the light state. The light states are not used in the combination difference analysis, and therefore the errors were smaller in those calculations. The optimized excited state rotational constants are presented in Table 3. Once the ground and excited state rotational constants were determined, the rotational temperature was determined to be 4 ± 1 K. Figure 8 shows a comparison of the bar graph representation of the original spectrum and the final calculated fit to the spectrum. Figure 9a shows a much smaller spectral region of the bar graph representation of the data containing several clusters of peaks. In figure 9b, the clusters of peaks have been reduced to single transitions to light states as described above. Finally, Figure 9c shows the calculated fit the to the spectrum. This sequence of spectra is typical of the correlation between the calculate fit to the data and the deconvolution of the clusters into transitions to the light states. Table 4 contains the frequencies of the deconvolved transitions to light states, the frequencies of the corresponding transitions in the calculated fit to the data and the difference between these two frequency values.

DISCUSSION

Coupling Matrix Elements:

A great deal of insight may be gleaned from the magnitudes and variation of the coupling matrix elements. From Table 2 it is apparent that the coupling matrix elements are not constant either within a single cluster of peaks or among different clusters. The implication of the variation in the matrix elements is that there is varying amounts of coupling between a given light state and various dark states. Notice, for example the cluster of peaks for the transitions to 3_{03} where the state is labeled by it's J and K quantum numbers as $J_{Ka,Kc}$. For this transition there are 4 peaks in the cluster, and the matrix elements range from 0.47×10^{-3} to 9.2×10^{-3} cm^{-1}. There is over an order of magnitude of variation in the size of these matrix elements. Thus, there is tremendous variation in the degree to which the 3_{03} state couples to neighboring states. Furthermore, no correlation was found in the frequency patterns and the matrix elements with the spacing of the dark states. One can only conclude that the mode-selectivity in the degree of coupling depends on the vibrational character of specific dark states.

Density of States:

Additional information about the mode-coupling is provided by examining the vibrational character of the states in the vicinity of the light state. The vibrational modes were identified by a state counting procedure that treats all, except two, of the vibrational modes as anharmonic oscillators. The anhamonicity of all vibrational modes was assumed to be 2%. Treating these modes as anharmonic rather than harmonic oscillators increased the density of states by less than 10%. The remaining two modes are the torsion about the C-C bond and the torsion about the C-O bond. These modes were treated as

hindered rotors using the well depths and potential barriers from literature values[5] and using a sum of cosines to approximate the hindered rotor potential surface[56]. The moments of inertia for the internal hindered rotation were held constant with respect to rotation and were treated as local rotors. These two approximations will overestimate the density of states in these modes. The density of states increased by a factor of 6 by treating these modes as hindered rotors rather than anharmonic oscillators. The resulting density of states is 63 states/cm^{-1} averaged over the frequency interval of 2980-2990 cm^{-1}.

The density of states can be used to estimate the fraction of dark states that couple with any given light state. With 63 states/cm^{-1}, if every dark state is mixed with the light state, the minimum spacing between states would be, on average, 0.016 cm^{-1}. For an average cluster of peaks in the experimental spectrum, the spacing between peaks is 0.006 cm^{-1}, significantly less than 0.016 cm^{-1}. The anharmonicity only has a small effect on the density of states as described above. Furthermore, no more than 7 quanta of any of the anharmonic oscillators contribute to any of the states in the vicinity of the light state. Therefore, even with significantly more anharmonicity the density of states would not account for the close spacing of the peaks in the clusters. The approximations inherent in the hindered rotor state density calculation overestimates the density of states. Thus, there is a discrepancy between the calculated density of states and the experimental data.

Mechanism of Mode-Coupling:

The prediction of the state spacing above is based on the assumption that states which couple conserve spatial rotational angular momentum. In other words, only states with the same rotational quantum numbers couple. This assumption is valid if the mechanism for the coupling is anharmonic

coupling. If Coriolis coupling occurs, however, states of different values of K_a and K_c can couple. As angular momentum increases, more states would be available for coupling. Since the degree of Coriolis coupling is dependent on the angular momentum, the coupling matrix element should also increase with angular momentum. One possible measure of the correlation between the matrix element and the angular momentum would be a plot of J *vs* the average matrix element. Figure 10 shows shows such a plot. Also shown in the figure is a plot of J *vs* the number of peaks per cluster. The number of peaks per cluster is a measure of the effective density of states available for coupling. The dependence of either of these parameters on J is inconclusive. Correlations with other angular momentum quantum numbers were also explored and were found to be similarly inconclusive. There may be a slight J dependence, but the positive slope in either case is not statistically significant because of the large variations in the parameters. The apparent uncertainties in the data is inherent in the parameters because we are averaging parameters that have large variations. It should be emphasized that the uncertainties are not a result of the measurement but of the magnitude of the parameters themselves. Similar problems occur in the plot of the number of peaks per cluster versus J. The density of states is so small that variation in the number of peaks per cluster could result from random variation in the local density of states rather than from variation solely on J. Also, there is a large variation in the magnitude of the matrix elements in a single cluster because of mode-selectivity in the coupling, as discussed above. If we could identify the particular modes that contribute to the particular peaks in a cluster, then the we could compare the magnitude of the coupling of that specific mode as a function of J. This kind of comparison would be more meaningful and could provide insight into the mechanism of coupling. To assist in the identification

of specific vibrational modes, experiments on deuterated 2FE are currently underway in our laboratory. By deuterating the OH in 2FE, modes that include motion of the OH bond will be perturbed with respect to other vibrations and should provide some information to help identify particular modes. Local variations in the density of states should also be apparent in the comparison of the spectra of the deuterated and undeuterated species.

Additional information regarding the mechanism of mode-coupling is derived from an examination of one specific transition in the spectrum. The transition in question is the transition to the $J_{Ka,Kb} = 0_{0,0}$ excited state. Coriolis coupling would predict no coupling in the 0_{00} state, while anharmonic coupling is independent of J. Because of the angular momentum selection rules, there is only one transition in the spectrum that occurs to the 0_{00}, namely the $0_{00} \leftarrow 1_{10}$. With only one transition, we cannot definitively identify a cluster in the spectrum associated with this transition. After fitting the spectrum, however, we examined the region where this transition is predicted to occur. This spectral region is shown in Figure 11, where the experimental data is shown in part a and the calculated fit to the data is shown in part b. Clearly from Figure 11, there is not one peak to associate with the predicted transition. Instead, we attribute the four labeled peaks in Figure 11a to a cluster of peaks. Using these peaks and determining the location of the light state as above results in remarkable agreement with the calculated fit to the data. The location and intensity of this light state is shown in Figure 11c. The matrix elements are given in Table 2. By comparison with other clusters, the magnitude of the matrix elements are large, implying a large degree of coupling in the 0_{00} state. Thus, anharmonic coupling must be present. Anharmonic coupling, however, does not preclude the presence of Coriolis coupling as well.

To account for the discrepancy between the calculated density of states and

the spacing of peaks in clusters in the experimental data, one might suggest that Coriolis coupling exists in some form. Two possible models that incorporate Coriolis coupling in the coupling mechanism are: 1) direct Coriolis coupling and 2) indirect Coriolis coupling. Direct Coriolis coupling would exhibit a J dependence. It is possible that we cannot observe a J dependence within the uncertainties in the data as described above. Therefore, direct Coriolis coupling cannot be ruled out. Indirect Coriolis coupling is a mechanism that has been suggested by Perry and coworkers.[36] Perry and coworkers suggest that it is possible to anharmonically couple a single light state to other vibrational modes. These other vibrational modes could then couple via Coriolis coupling to a variety of other states, thereby increasing the number of peaks in a cluster. We cannot distinguish between these two scenarios with our data.

Previous experiments that studied vibrational coupling on similar sized molecules exhibit quite different coupling mechanisms.[36-39] Specifically, previous results on 1-butyne[38] and ethanol[36] suggest that the vibrational mode-coupling in these two molecules have different dependences on the J quantum number in the excited state. In 1-butyne, the results are very similar to those observed here for 2FE. Anharmonic coupling is present as evidenced by the presence of coupling in the J=0 excited state. Although there is not a strong dependence on J, Coriolis coupling cannot be ruled out, as in the results for 2FE. In contrast, for the case of ethanol, a strong dependence of the vibrational mode-coupling on J is observed. Thus, Coriolis coupling is clearly evident in ethanol. It is somewhat surprising, given the similarity of 2FE to ethanol, that the evidence of mode-coupling is so different.

Interesting comparisons between 1-butyne, ethanol and 2FE are also found in the magnitudes of the coupling matrix elements. The average matrix element in 2FE is a factor of 2-3 smaller than that of 1-butyne and more than a

factor of 2 smaller than that of ethanol. The C-H stretch of the 1 carbon in 1-butyne would be expected to couple particularly poorly to the rest of the modes in the molecules, as noted by the authors.[38] The coupling matrix element is expected to be small in 1-butyne, yet the magnitude of the coupling in 2FE is a factor of 2-3 smaller. The similarity of the structure of 2FE and ethanol would suggest that the coupling should be of the same magnitude, yet again, the coupling in 2FE is at least a factor of 2 smaller. The surprisingly small amount of coupling must be a result of the difference in the structure between 2FE and ethanol. 2FE has intramolecular interactions that stabilize the Gg' form while in ethanol the lowest energy form is the trans form with the proton extended out away from the rest of the molecule. The strong attractive interactions must make the structure of the molecule significantly more rigid. This rigidity would tend to lock in the conformation of the molecule making the low energy torsional modes less accessible for coupling. This qualitative physical picture of the molecular structure would also account for the observed difference in magnitude of coupling between 2FE and 1-butyne. In 1-butyne, although the C-H stretch is inhibited from coupling to the rest of the molecule via a triple bond, the rest of the molecule consists of a floppy tail that provides accessible torsional modes. Closer inspection of the types of vibrational modes that couple to the light state is necessary to develop a picture of mode-coupling.

Although identification of the modes that make up specific dark states is not possible from the data, important information is derived from an examination of the composition of the vibrational modes in the 10 cm^{-1} vicinity of 2980 cm^{-1}. As noted above, the density of states dramatically increases when the torsional modes are treated as hindered rotors. It is not surprising, therefore to discover that 99 % of the dark states are combination bands that contain at least one quantum of one of these torsional modes

Several of the dark states contain over 40 quanta of the C-C torsion. Assuming that the degree of Coriolis coupling is small, virtually all of the dark states in the vicinity of the light state must be coupled in order to account for all of the transitions in the spectrum. From identification of these states, virtually all contain some component of torsional vibration. Therefore, the molecular eigenstates all contain a significant component of torsional vibration as well as asymmetric C-H stretching vibration. If the torsional vibrations do not couple well to the asymmetric stretch, then one would expect the coupling matrix elements to be small as determined by the experiment.

Mode-Selective Chemistry:

The results of the experiment presented here provides new insight into the mode-selective reaction rates for conformational photoisomerization observed in low temperature matrix experiments.[17] The matrix experiments are fundamentally different from the present high resolution experiments. In these high resolution experiments excitation occurs to the molecular eigenstates. In contrast, in the matrix experiments a superposition state is excited. The superposition state may be thought of as the C-H asymmetric stretching normal mode that contains all of the oscillator strength--the light state. This state evolves in time as the energy flows from the C-H stretch into the reactive coordinate, the torsional modes. The timescale of this state evolution depends on the amount of coupling between the light state and the reactive coordinate. The coupling is given by the matrix element determined from our high resolution experiment. As noted above, the rate of photoisomerization was observed to be 5 times slower when the asymmetric C-H stretch was excited than when the O-H stretch was excited.[17] The fact that the matrix element is small in magnitude is completely consistent with the fact

that the reaction rate is small when the C-H stretch is excited. Thus, these high resolution results supports the conclusion that mode-selective chemistry is responsible for the variation in the reaction rates observed in the matrix experiments. Further evidence in support of these conclusions would be provided by examination of the mode-coupling in the O-H stretching region via high resolution spectroscopy. Such experiments are currently underway in our laboratory. Careful preliminary examination of the O-H region have been unsuccessful in finding any peaks. Since all experimental parameters are the same as those used in the C-H region, the peaks are likely to be too small to be detected with the current experimental sensitivity. Peaks that are significantly smaller than those in the C-H region would indicate significantly more mode-coupling for the O-H stretch. Again, this trend would be consistent with concluding that mode-selective chemistry is responsible for the discrepancy in the reaction rates. Until the spectrum of the O-H stretching region has been measured, however, such conclusions should be viewed with caution.

Molecular Geometry:

A possible geometry for 2-fluoroethanol was determined from the rotational constants for both the ground and excited vibrational states. The rotational constants for the ground state are consistent with Gg' geometry. A reasonable ground state geometry was determined starting with the microwave structure, and modifying the structure until agreement with the rotational constants was achieved to within 0.7%. The modifications were guided by *ab initio* calculations using the Gaussian88 package, with both STO3-G and 4-31G basis functions, on the Cornell National Supercomputer. To determine a structure for the excited state we calculated a geometry that is consistent with the measured change in the rotational constants from the ground state to the

excited state. The Gg' geometry of the ground state was used as a starting point and the bond lengths for the C-H bonds of the fluoronated carbon were modified. It is these bonds that we expect to exhibit the most dramatic change upon excitation of a vibrational mode that is dominantly asymmetric C-H stretch. These modifications alone, however, do not account for the observed changes in the rotational constants. If a small amount of C-C torsion (2%) is added the calculated rotational constants are consistent with the experimental values within experimental uncertainties. It should be emphasized that with only three rotational constants, it is impossible to completely determine the geometry of the excited state. The proposed geometry is merely physically reasonable and consistent with the model of vibrational mode-coupling described above.

Further evidence of the excited state geometry is found in the direction of the transition moment. The ground state and excited state dipole moments were calculated using HONDO8 with 4-31G basis functions. The dipole moment was also determined for a variety of different excited state geometries. By vector addition, the transition moment direction was then determined. A 1% change in the C-H bonds on the fluorinated carbon does not result in a predominantly C type transition. In fact with modification of the C-H bonds alone, predicts at most 60% C type. A small addition C-O torsion(0.2%) results in an improvement to 73% C type transition. Once again, although this excited state geometry is not a unique fit to the experimental parameters, it is consistent with the experimental data and consistent with the mode-coupling arguments.

CONCLUSIONS

High resolution infrared spectroscopy in a molecular beam has proven to be a powerful tool to examine the structure and dynamics of 2FE. The spectrum of the asymmetric CH stretch in 2FE has definitive evidence of the existence of vibrational mode-coupling. The mode-coupling was measured quantitatively from the location and intensities of transitions that make up clusters of peaks in the spectrum. The magnitude of the mode-coupling varied dramatically within individual clusters of peaks as well as between different clusters. This variation in mode-coupling demonstrates that there is mode-selectivity in the mode-coupling. The actual mechanism of mode-coupling cannot be determined conclusively from the data, however, there is some evidence for both anharmonic and Coriolis coupling. Further experiments are necessary to provide more information about the coupling mechanism. Comparison with previous high resolution experiments on similar molecules suggest that the amount of mode-coupling in 2FE is exceptionally small. Such limited mode-coupling is consistent with the slow conformational isomerization rates observed in low temperature matrix experiments. Furthermore, these results suggest a correlation between the isomerization rate and the magnitude of vibrational mode-coupling, and support the model of mode-selectivity in the isomerization rates. We suggest that the minimal amount of mode-coupling is related to the strong intramolecular attractive interactions in 2FE, which act to inhibit coupling between the torsional reaction coordinate and the asymmetric CH stretch. Clearly further high resolution experiments on related molecules, as well as other vibrational modes in 2FE would provide invaluable data to test these conclusions and provide more insight into the connection between vibrational mode-coupling and chemical reactivity.

Acknowledgement: This work is supported by: The National Institute of Health under grant #08-R9N527039A; The Office of Naval Research under grant #N00014-90-J-1971; The Petroleum Research Fund, administered by the American Chemical Society; The National Science Foundation under grant #89-10583; and Proctor and Gamble. The authors gratefully acknowledge the assistance of Julian M. Hjortshoj, C. Cameron Miller and Kevin B. Hewett in the data analysis portion of the research. The authors would also like to thank G. Fraser for many helpful discussions.

REFERENCES

1. H. Frei, G. C. Pimentel, Ann. Rev. Phys. Chem., **36**, 491 (1985), and references therein.

2. K. S. Buckton, R.G. Azrak, *J. Chem Phys.*, **52**, 5652 (1970).

3. K. Hagen, K. Hedberg, *J. Am. Chem. Soc.*, **95**, 8263 (1973); J. Huang, K. Hedberg, *J. Am. Chem. Soc.*, **111**, 6909 (1989).

4. G. Alagona, R. Bonaccorsi, C. Ghio, J. Tomasi, *J. Mol. Struct.* (Theochem), **137**, 263 (1986).

5. K.B. Wiberg, M. A. Murcko, *J. Mol. Struct.* (Theochem) **163**, 1 (1988).

6. W. F. Hoffman III, J. S. Shirk, *Chem. Phys.*, **78**, 331 (1983).

7. P. Buckley, P.A. Giguere, D. Yamamoto, *Can. J. Chem.*, **46**, 2917, (1968).

8. M. Rasanen, J. Murto, V. E. Bondybey, *J. Phys. Chem.*, **89**, 3967(1985).

9. D.A. Dixon, B.E. Smart, *J. Phys. Chem.*, **95**, 1609 (1991).

10. R. G. Azrak, E.B. Wilson, *J. Chem. Phys.*, **10**, 5299 (1970).

11. E. Lombardi, G. Tarantini, *Chem. Phys, Lett.*, **60**, 85 (1978).

12. J. Pourcin, G. Davidovics, H. Bodot, L. Abouaf-Marguin, B. Gauthier-Roy, *J. Mol. Spect.*, **109**, 186 (1985).

13. J. Pourcin, M. Monnier, P. Verlaque, G. Davidovics, R. Lauricella, C. Colonna, H. Bodot, *Chem. Phys. Let.*, **74**, 147 (1980).

14. Z. H. Kafafi, C. L. Marquardt, J. S. Shirk, *J. Chem. Phys.*, **90**, 3087 (1989).

15. M. Perttila, J. Murto, A. Kivinen, *Spect. Acta*, **34A**, 9 (1978).

16. J. S. Shirk, C. L. Marquardt, *J. Chem. Phys.*, **92**, 7234 (1990).

17. O. Schrems, *Ber. Bunserges Phys. Chem.*, **89**, 297 (1985).

18. W. F. Hoffman III, J. S. Shirk, *J. Phys. Chem.*, **89**, 1715 (1985).

19. P.J. Kruger, H.D. Mettee, *Can. J. Chem.*, **42**, 326 (1964).

20. E.A. Robinson, H.D. Schreiber, J.M. Specer, *Spectrochim. Acta*, **28A**, 397 (1972).

21. D. Davenport, M. Schwartz, *J. Mol. Struct.*, **50**, 259 (1978); A. Gupta, D. Davenport, M. Schwartz, *Spectrochemica Acta*, **36A**, 601 (1980).

22. R. Meyer, M. Pertlila, *J. Mol. Struct.*, **64**, 1 (1980).

23. R. Gunde, A. Azman, *J. Mol. Struct.*, **27**, 212 (1975).

24. J. Murto, M. Rasanen, A. Aspiala, L. Homanen, *J. Mol. Struct.*, **92**, 45 (1983).

25. G. Davidonics, *J. Mol. Struct.*, **99**, 165 (1983).

26. G. Davidovics, *J. Mol. Struct.*, **116**, 39 (1984).

27. O. Schrems, W.A.P. Luck, *J. Mol. Struct.*, **80**, 477 (1982).

28. K.G.R. Pachler, D.L. Wessels, *J. Mol. Struct.*, **6**, 471 (1970).

29. E. Wyn-Jones, W.J. Orvillet-Thomas, *J. Mol. Struct.*, **1**, 79 (1967).

30. O. Schrems, H. M. Oberhoffer, W. A. P. Luck, *J. Mol. Struc.*, **80**, 129 (1982).

31. J. Murto, M. Rasanen, A. Aspiala, T. Latta, *J. Mol. Struct.* (Theochem), **108**, 99 (1989).

32 S.M. Craven, F.F. Bentley, *Applied Spec.*,, **26**, 242 (1972).

33. J. Kommandeur, W.A. Majewski, W.L. Meerts, D.W. Pratt, Ann. *Rev. Phys. Chem.* **38**, 433 (1987).

34. A. M. de Souza, D. Kaur, D. S. Perry, *Ber. Buns. Phys. Chem.*, **92**, 424 (1988).

35. A. M. de Souza, D. Kaur, D. S. Perry, *J. Chem. Phys.*, **88**, 4569 (1987).

36. J. Go, G.A. Bethardy, D.S. Perry, *J. Phys. Chem.*, **94**, 6153 (1990).

37. A. McIlroy, D. J. Nesbitt, *J. Chem. Phys.*, **91**, 104 (1989).

38. A. McIlroy, D. J. Nesbitt, *J. Chem. Phys.*, **92**, 2229 (1990).

39. C. L. Brummel, S. W. Mork, L. A. Philips (accepted, *J. Am. Chem. Soc.*).

40. C. M. Lovejoy, M. D. Schuder, D. J. Nesbitt, *Chem. Phys. Lett.*, **127**, 374 (1986); C. M. Lovejoy, M. D. Schuder, D. J. Nesbitt, *J. Chem. Phys.*,**85**, 4890 (1986).

41. R. E. Miller, *J. Phys. Chem.*, **90**, 3301 (1986), and references therein.

42. D. J. Nesbitt, *Chem. Rev.*, **88**, 843 (1988).

43. T. E. Gough, R. E. Miller, G. Scoles, *App. Phys. Lett.*, **30**, 338 (1977); T. E. Gough, R. E. Miller, G. Scoles, *J. Phys. Chem.*, **85**, 4041 (1981).

44. Z. S. Huang, R. E. Miller, *J. Phys. Chem.*, **92**, 46 (1988); Z. S. Huang, K.W. Zucks, R. E. Miller, *J. Chem. Phys.*,**85**,3338 (1986); *J. Chem.Phys.*, **86**, 1098 (1987).

45. D. F. Coker, R. E. Miller, R. O. Watts, *J. Chem. Phys.*, **82**, 3554 (1985); G. Fischer, R. E. Miller, P. F. Vohralik, R. O. Watts, *J. Chem. Phys.*, **83**, 1471 (1985); K. G. H. Baldwin, R. O. Watts, *J. Chem. Phys.*, **86**, 1225 (1987); Z. S. Huang, R. E. Miller, *J. Chem. Phys.*, **89**, 5408 (1988).

46. C. V. Boughton, R. E. Miller, R. O. Watts, *Aust. J. Phys.*, **35**, 611 (1982).

47. A.S. Pine, G.T. Fraser, *J. Chem. Phys.*, **89**, 100 (1988).

48. G.T. Fraser, A.S. Pine, W.J. Lafferty, R.E. Miller, *J. Chem. Phys.*, **87**, 1502 (1987).

49. C.L. Morter, A. Koskelo, Y.R. Wu, D.H. Levy, *J. Chem. Phys.*,**89**, 1867 (1988); C.A. Haynam, C.L. Morter, L. Young, D.H. Levy, *J. Phys. Chem.*,**91**, 2519 and 2526 (1987).

50. D. H. Levy, C. A. Haynam, D. V. Brumbaugh, *Faraday Discuss. Chem. Soc.*, **73**, 137 (1982); *J. Mol. Spec.*, **94**, 316 (1982); D. V. Brumbaugh, J. E. Kenny, D. H. Levy, *J. Chem. Phys.*, **78**, 3415 (1983).

51. L. A. Philips, D. H. Levy, *J. Phys. Chem.*, **90**, (1986).

52. L.A. Philips, D.H. Levy, *J. Chem. Phys.* **88**, (1988).

53. L. A. Philips, D. H. Levy, *J. Chem. Phys.*, **85**, 1327 (1986).

54. Program written by A. Maki and furnished to us by G. T. Fraser, N.I.S.T., Gaithersberg, MD, 20899.

55. W.D. Lawrence, A.E.W. Knight, *J. Phys. Chem.*, **85**, 917 (1985).

56 J.D. Lewis, T.B. Malloy, Jr., T.H. Chao, J. Lanne, *J. Mol. Struct.*, **12**, 427 (1972)..

FIGURE CAPTIONS

1. The schematic diagram above depicts the conformational isomerization coordinate, for the Gg' to Tt isomerization. The barrier heights and relative stability of the two conformations are based on literature values (see refs. 3-7). Notice that the Gg' conformation is substantially more stable than the Tt conformation, in spite of the reduced steric crowding in the Tt conformation.

2. The experimental apparatus is shown diagramatically above. In the figure the following abbreviations are used: E - etalon; K - kinematically mounted mirror; C - chopper; D - detector for monitoring the power; L - lens; W - wavemeter; B - bolometer. The two etalons are a scanning etalon and a fixed etalon for frequency calibration as described in the text.

3. The spectral region shown above contains a single peak as measured when the laser beam crosses the molecular beam at a right angle. To achieve optimal resolution the laser beam is crossed with the molecular beam a single time. The peak is fit to both a Lorentzian and a Gaussian lineshape. The Gaussian profile clearly is a better fit to the data and gives an experimental linewidth of 7 MHz.

4. The data that is acquired during a scan is shown in the four traces above. Trace D is the raw experimental spectrum. Traces A and C are the output from the two etalons, used for frequency calibration, as described in the text. Trace B is the output from a detector that monitors the laser power.

5. Once the data has been reduced to a two dimensional array containing the position and intensity of the individual peaks, the data is represented as shown above in a bar graph plot. The position of the lines correspond to the normalized frequency of the peaks and the height of the lines represent their normalized intensity.

6. Part A above, represents a diagram of zeroeth order eigenstates. The figure shows transitions from two different rotational states in the ground vibrational state that occur to the same excited ro-vibrational state. The vibrational excited state represents the single vibrational state that carries oscillator strength in the zeroeth order approximation. In addition to this excited state, there exists a manifold of dark states, states that have little or no oscillator strength in the zeroeth order approximation. Part B depicts what happens when the zeroeth order picture is perturbed and the excited vibrational states become mixed. The spectrum in the zeroeth order picture would consist of two single peaks. The spectrum in the perturbed picture would consist of two clusters of peaks with identical frequency and intensity patterns. The true molecular eigenstates correspond to the perturbed picture.

7. Each panel in the figure shows two sets of transitions to the same excited state. The transitions are labeled with the J and K_a and K_c quantum numbers as J_{K_a,K_c} corresponding to the labels of the zeroeth order uncoupled states. The left panel shows two sets of transitions to the 1_{10} excited state. The middle and right panels are transitions to the 2_{02} and 3_{12} excited states respectively. In each case the similarity of the patterns of peaks positions and intensities are apparent, demonstrating the presence of vibrational mode-coupling.

8. The bottom panel of the figure shows the reduced data as in Figure 5. The top panel is a similar depiction of the best calculated fit to the data. The calculated fit is performed using a rigid rotor asymmetric top model. Notice that there are many more peaks in the experimental data than in the calculated fit. The additional peaks are due to the presence of mode-coupling in the data that is not accounted for in the calculation.

9. The figure shows the reduced data in a small region of the spectrum. Panel A is the bar graph representation of the data. In panel B, the clusters of peaks have been deconvolved into a single light state for each cluster by the technique described in the text. Panel C shows the calculated fit to the data. Notice the remarkable correlation between the deconvolved data and the calculated fit to the data.

10. Both the coupling matrix elements and the peaks per cluster are plotted as a function of the rotational quantum number J. (+) are the average of the number of peaks per cluster for all of the clusters with a given quantum number. Similarly, (●) are the average values for all of the peaks in all of the clusters for a given value of the J quantum number. Each J quantum number represents various contributions from a range of different excited states, with one exception. There was only one excited state that had J=5. The inherent uncertainties in the plotted values are substantial as discussed in the text.

11. The single transition to the 0_{00} in the excited state is shown above in panel A. The labeled peaks are used in the deconvolution process described in the text to determine the position of the light state. The position and intensity of the light state is shown in panel B. In panel C is shown the position and intensity of the corresponding peak in the calculated spectrum.

TABLES

Table 1: Frequency and intensity of the peaks in the spectrum labeled with the appropriate quantum numbers for the ground and excited states of each transition

Table 2: Column 1 gives the quantum number of the excited state. In column 2 is the position of each dark state with respect to the light state in a given cluster of peaks. In column 3 is the coupling matrix element that describes the coupling between the light state (L) and each dark state (D).

Table 3: The first 2 columns present the excited state and ground state quantum numbers for each transition. Column 3 gives the position of the light state as determined from each cluster of peaks. In column 4 is the deviation of the position of the corresponding calculated peak from the position of the light state.

Table 4: The parameters used to calculate the best fit to the experimental data using a rigid rotor model.

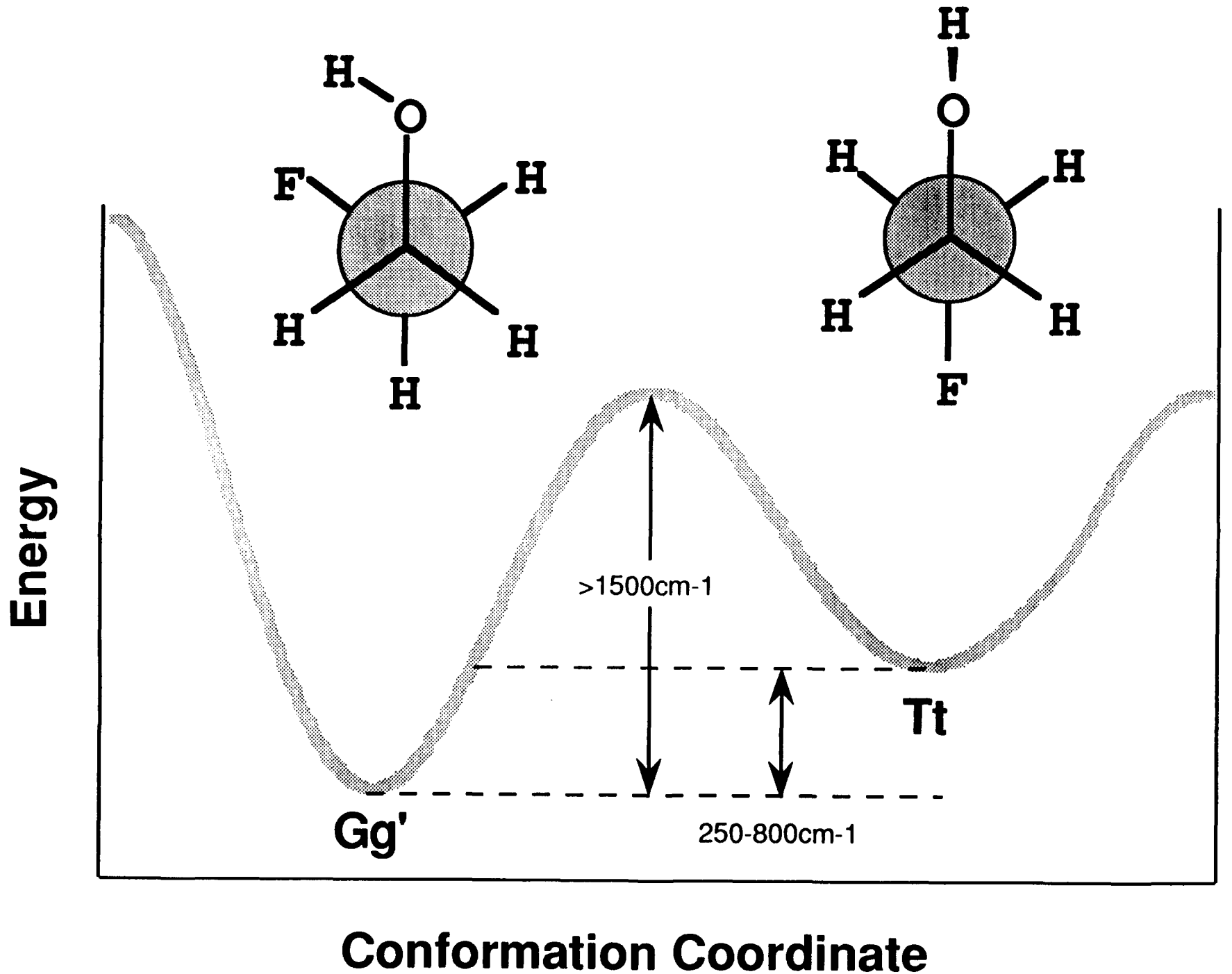
H
O
F
H
H
H
H
H
H
H
H
H
O
H
H
H
F
Energy
>1500cm-1
Tt
Gg'
250-800cm-1
Conformation Coordinate

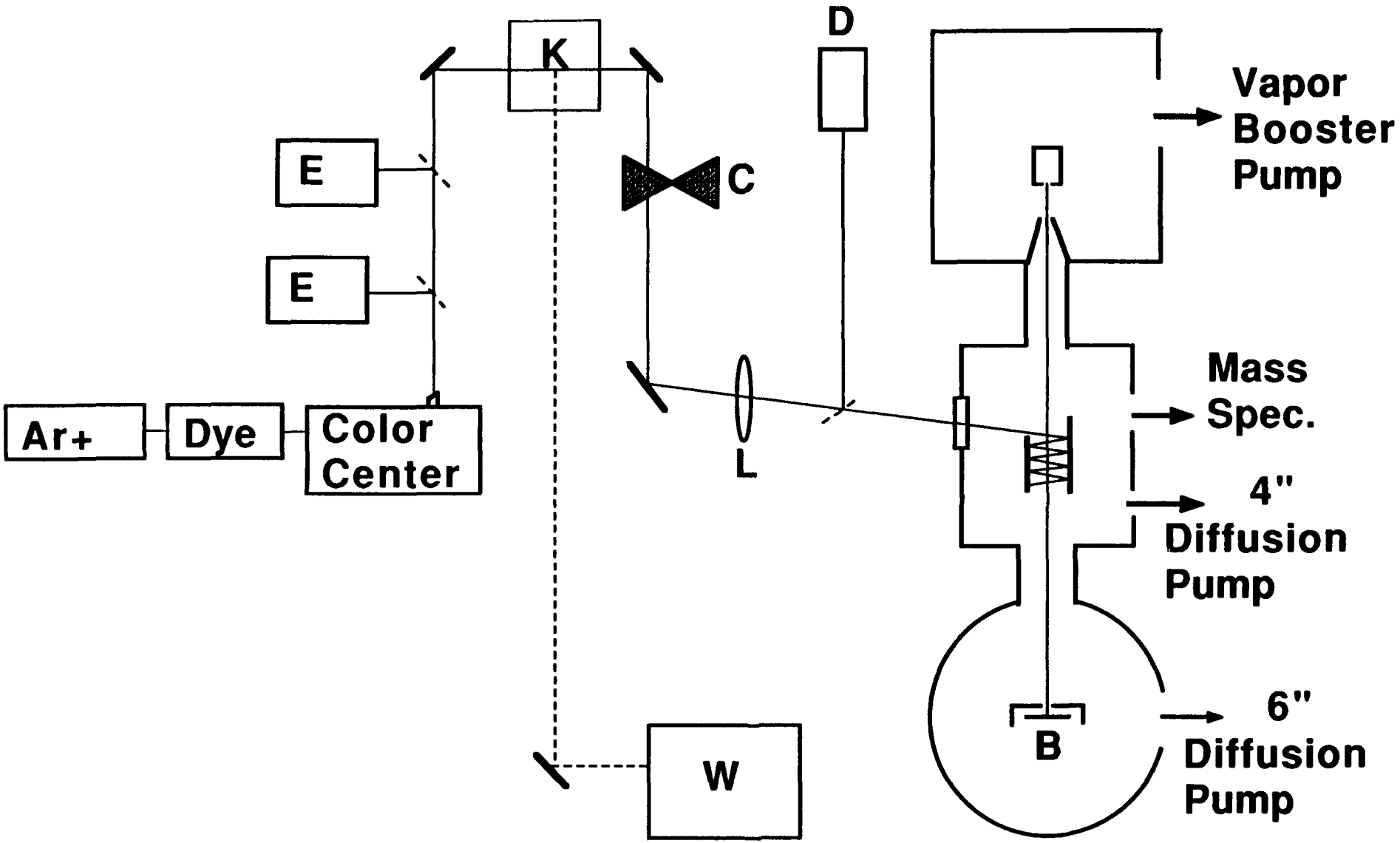
K
D
E
C
E
Vapor
Booster
Pump
Ar+
Dye
Color
Center
L
Mass
Spec.
4"
Diffusion
Pump
B
6"
Diffusion
Pump
W

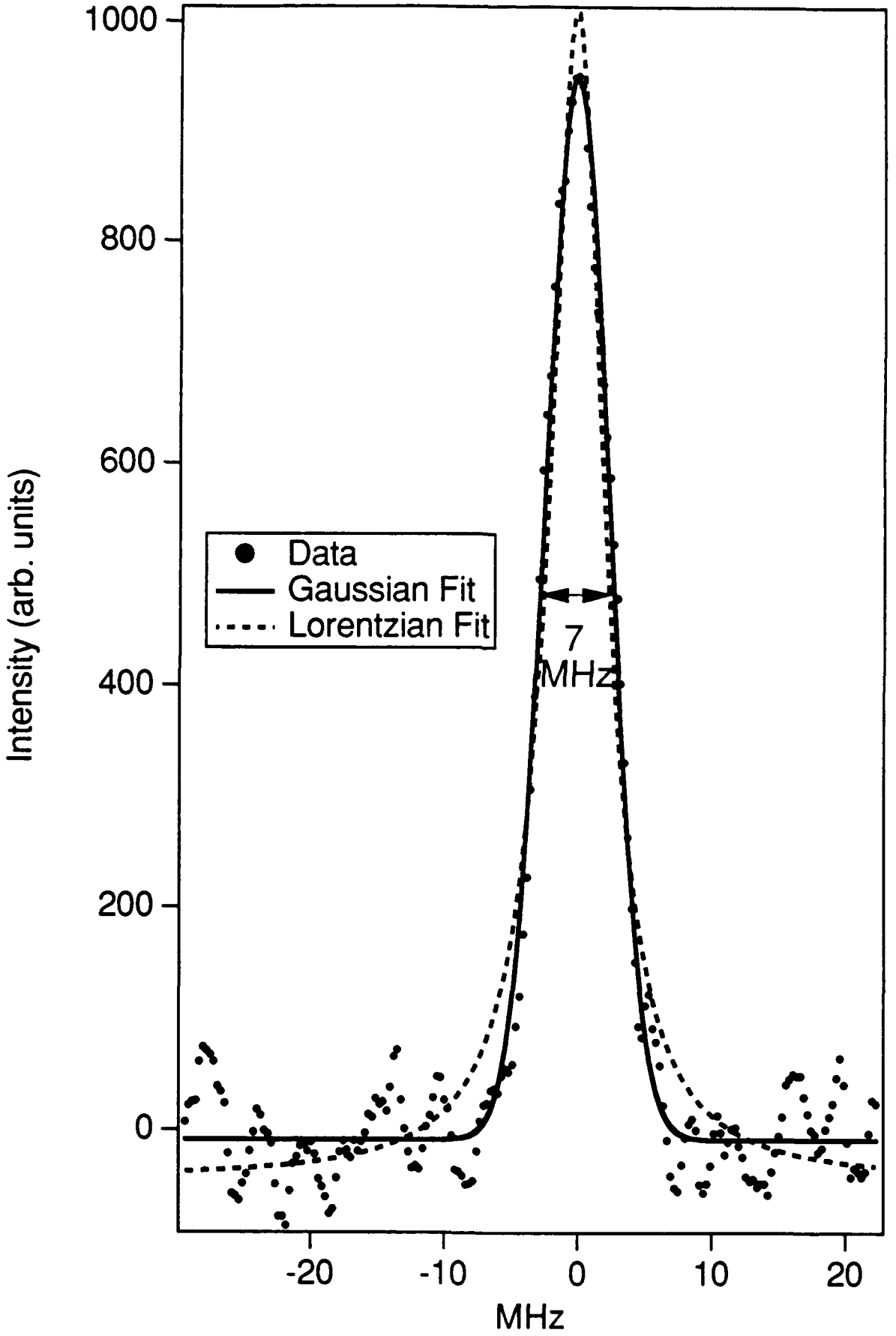
1000
800
600
400
200
0
Intensity (arb. units)
Data
Gaussian Fit
Lorentzian Fit
7
MHz
-20
-10
0
10
20
MHz

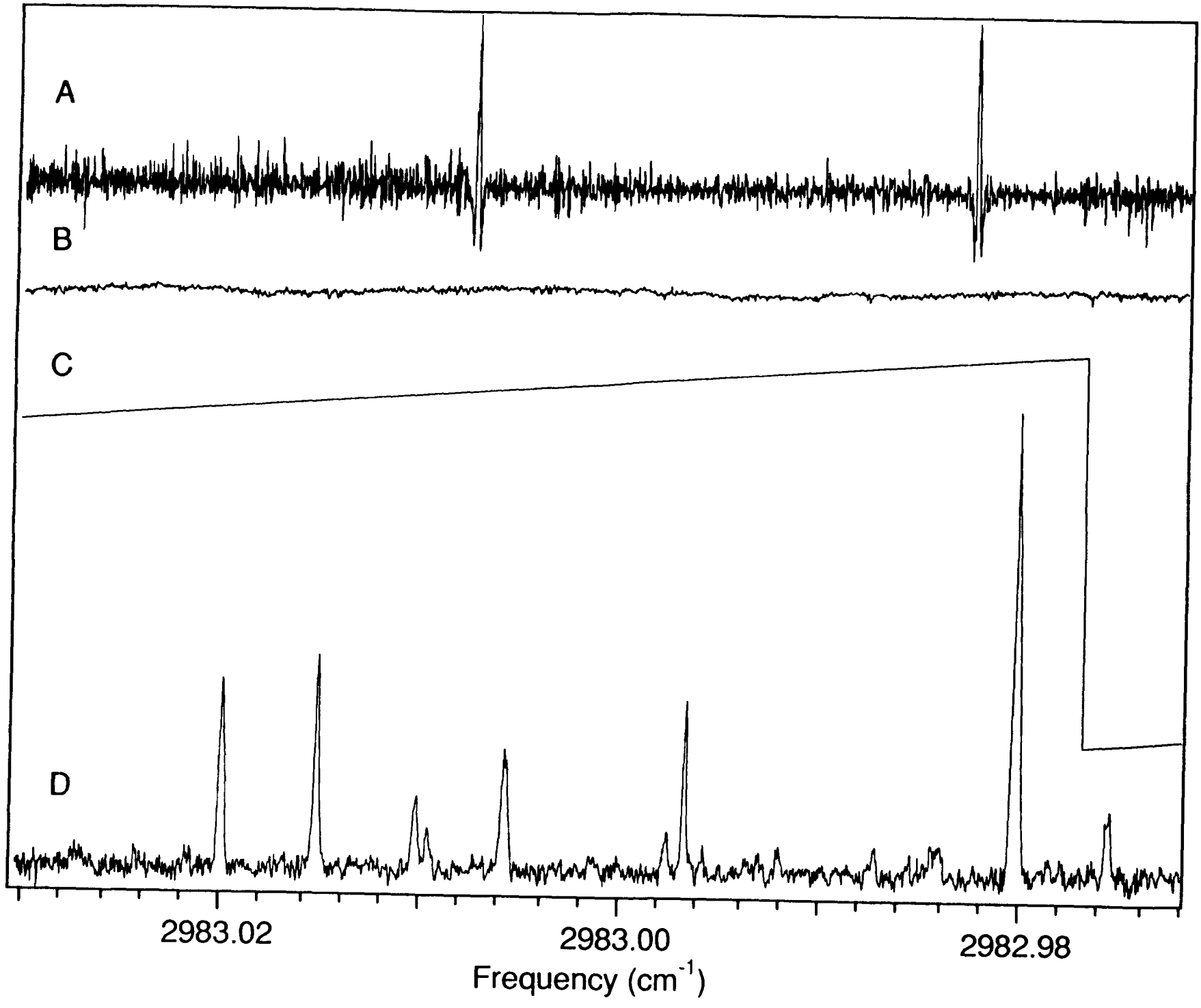
A
B
C
D
2983.02
2983.00
2982.98
Frequency (cm-1)

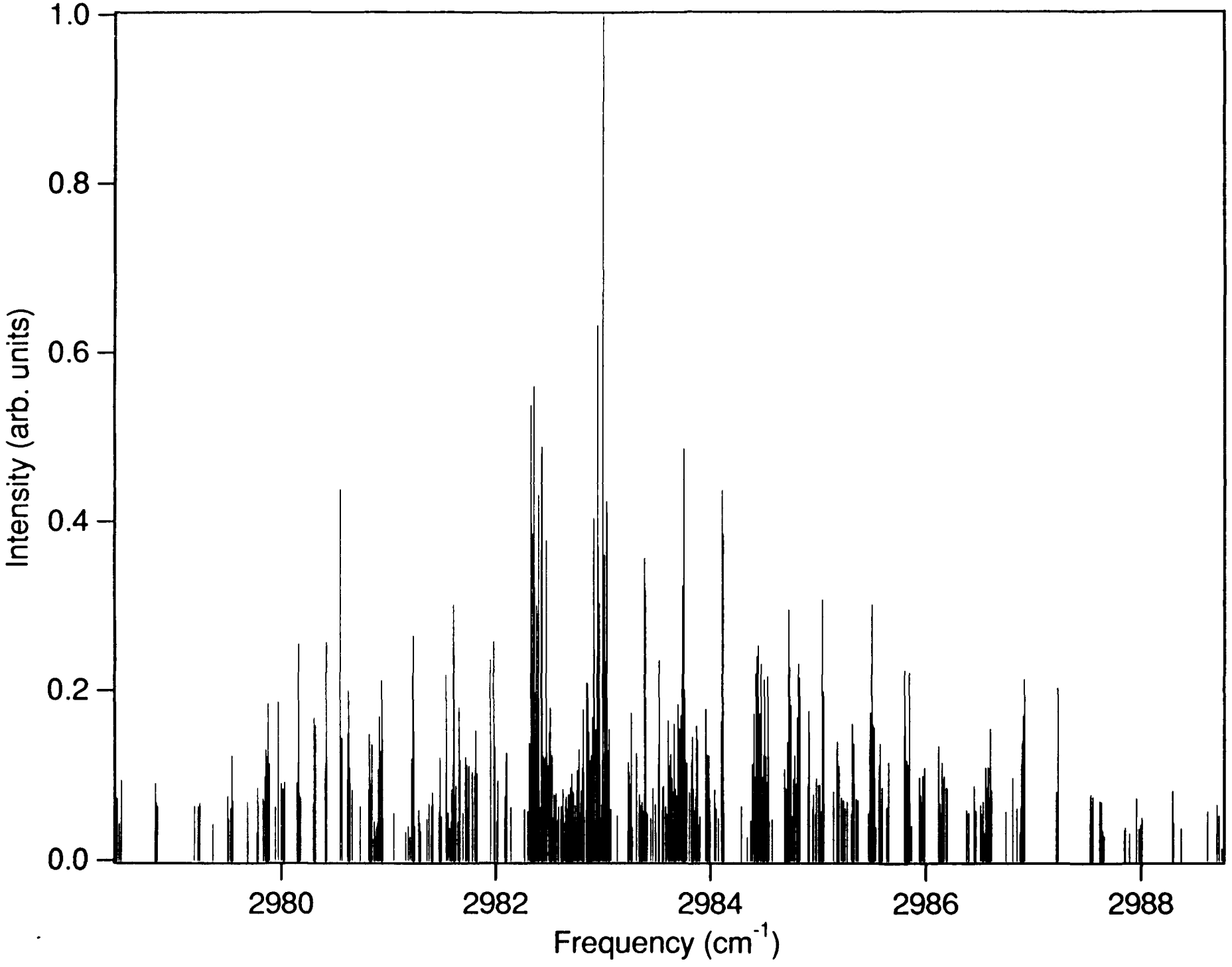
1.0
0.8
0.6
0.4
0.2
0.0
Intensity (arb. units)
2980
2982
2984
2986
2988
Frequency (cm-1)

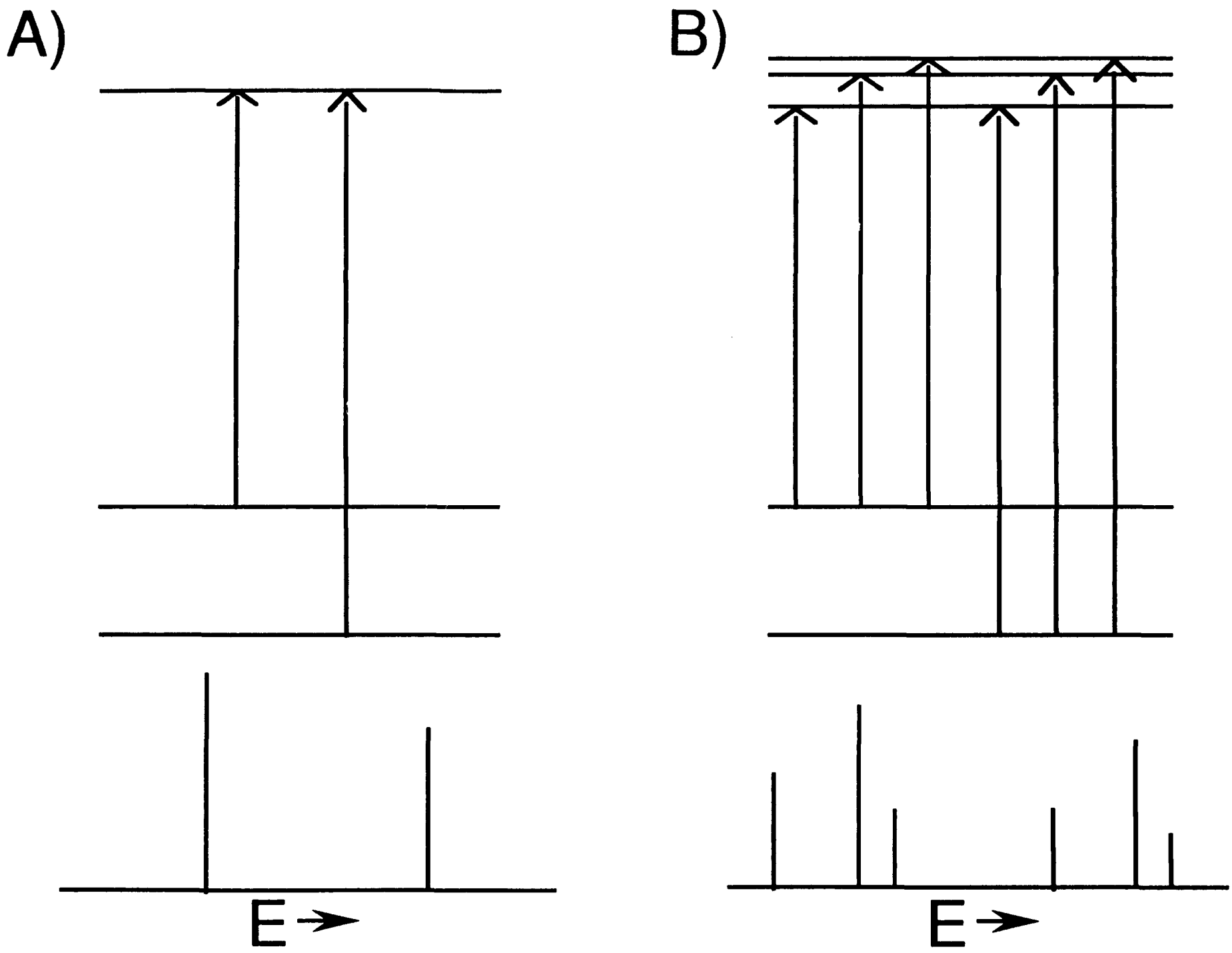
A)
B)
E
E

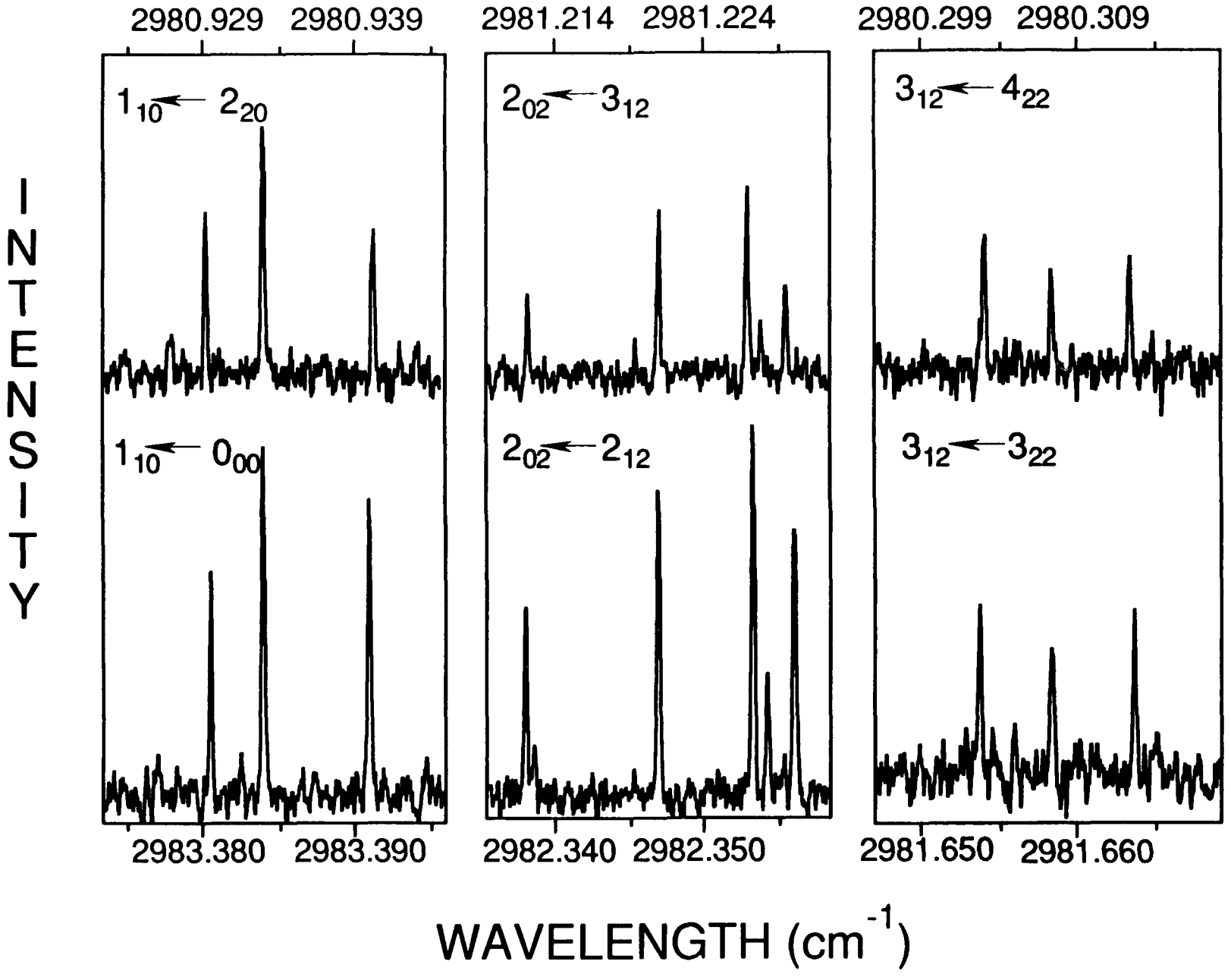
2980.929
2980.939
2981.214
2981.224
2980.299
2980.309
$1_{10} \leftarrow 2_{20}$
$2_{02} \leftarrow 3_{12}$
$3_{12} \leftarrow 4_{22}$
$1_{10} \leftarrow 0_{00}$
$2_{02} \leftarrow 2_{12}$
$3_{12} \leftarrow 3_{22}$
2983.380
2983.390
2982.340
2982.350
2981.650
2981.660
INTENSITY
WAVELENGTH (cm^{-1})

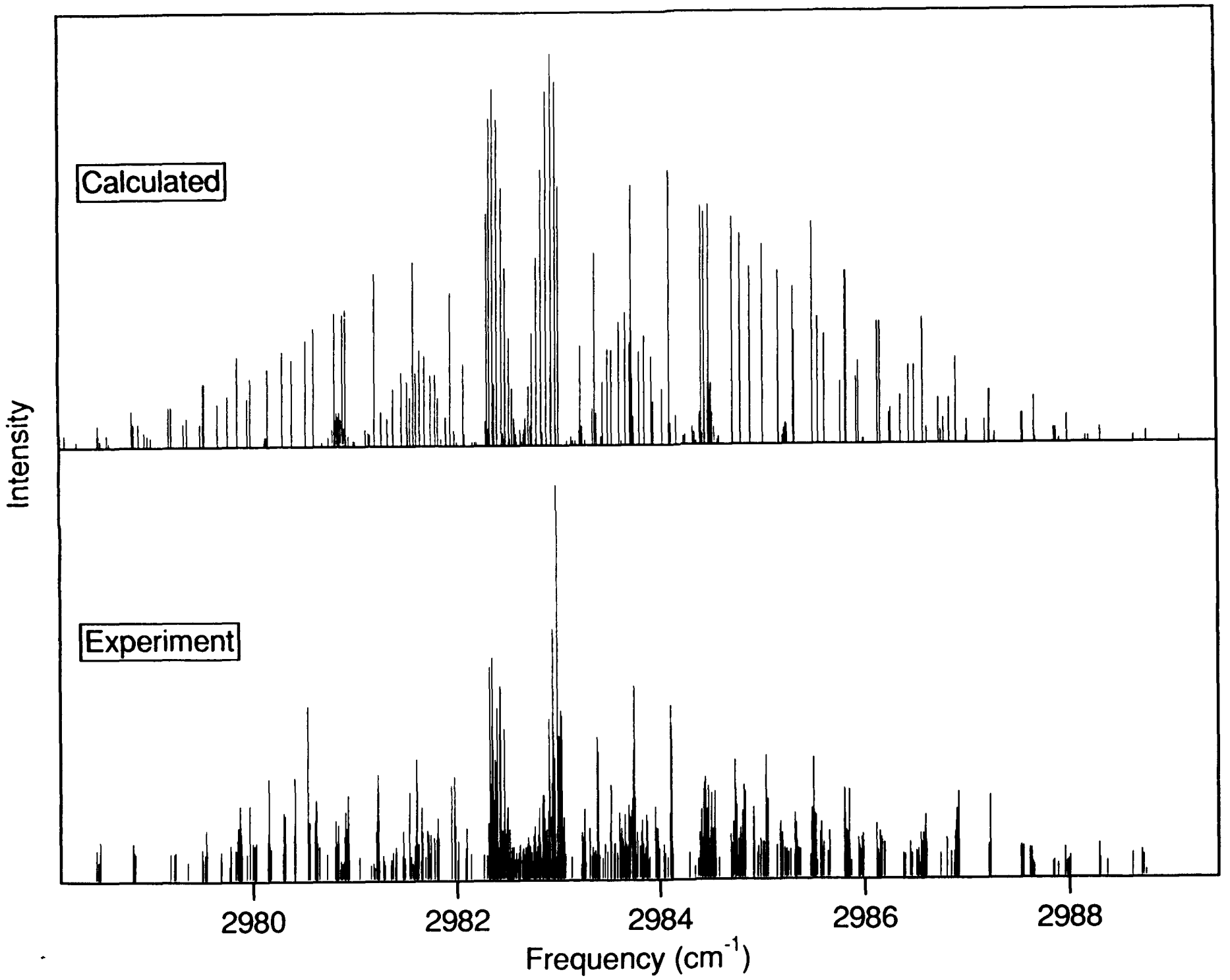
Calculated
Experiment
Intensity
2980
2982
2984
2986
2988
Frequency (cm-1)

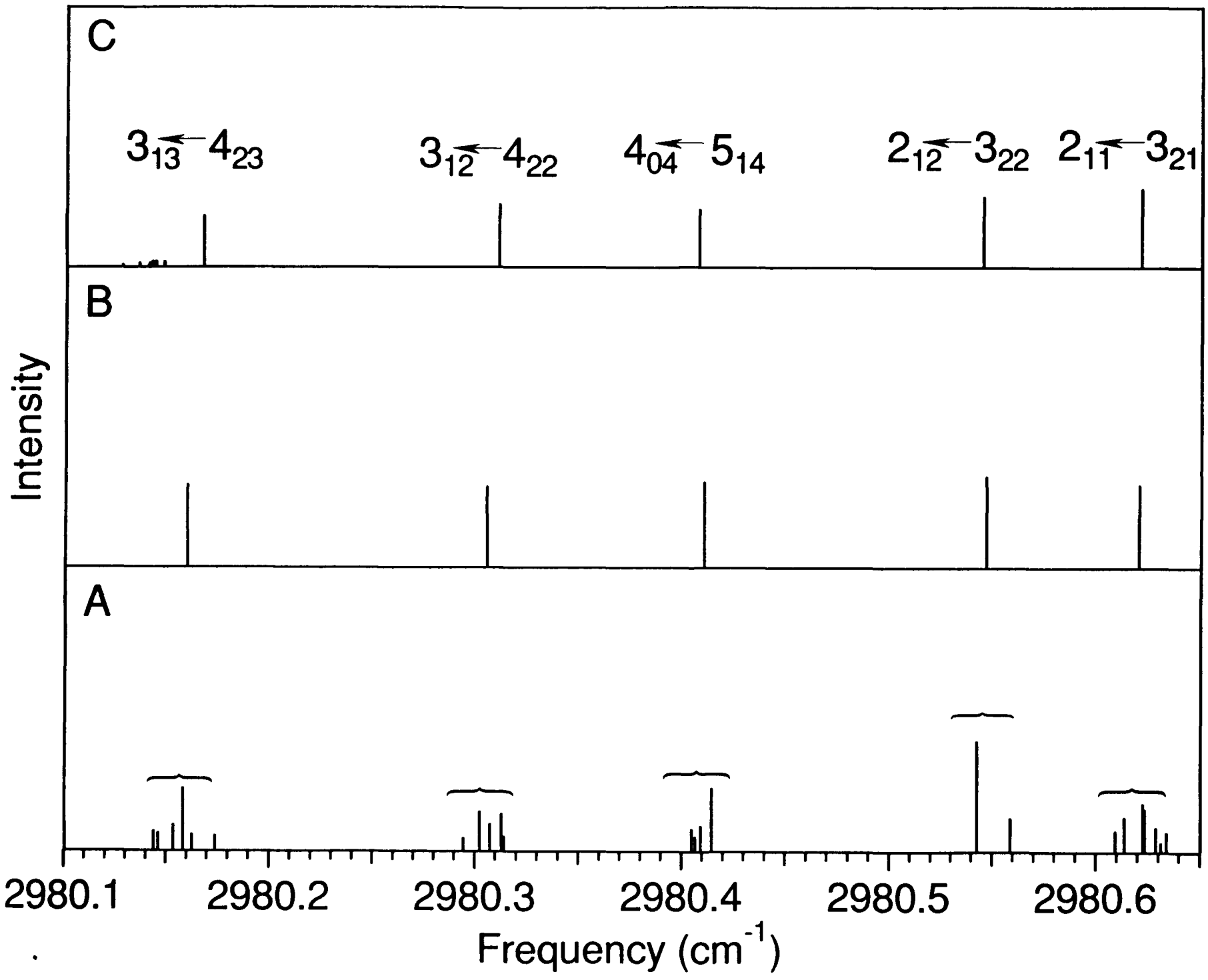
C
$3_{13} \leftarrow 4_{23}$
$3_{12} \leftarrow 4_{22}$
$4_{04} \leftarrow 5_{14}$
$2_{12} \leftarrow 3_{22}$
$2_{11} \leftarrow 3_{21}$
B
A
Intensity
2980.1
2980.2
2980.3
2980.4
2980.5
2980.6
Frequency (cm^{-1})

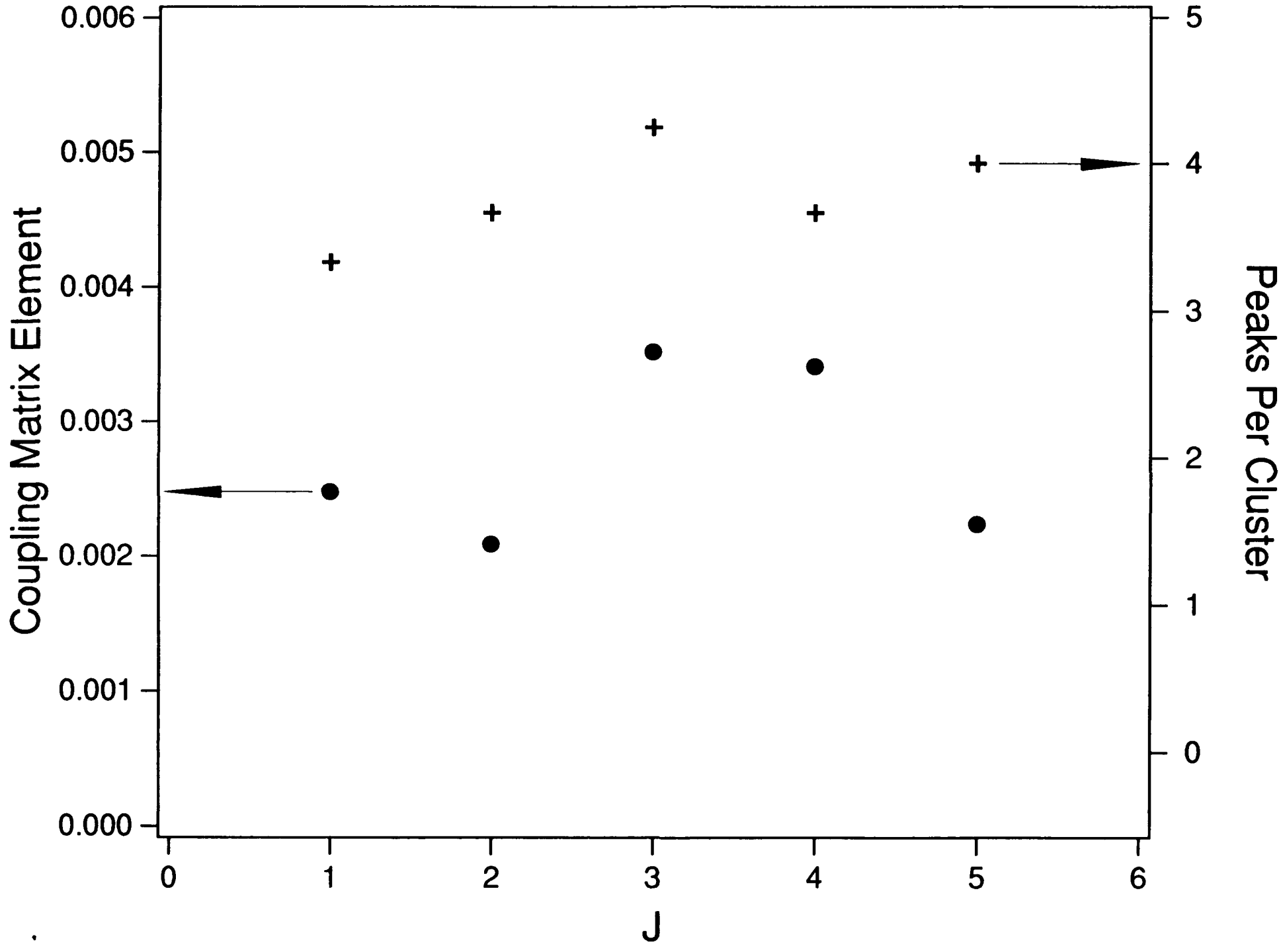
0.006
0.005
0.004
0.003
0.002
0.001
0.000
Coupling Matrix Element
5
4
3
2
1
0
Peaks Per Cluster
0
1
2
3
4
5
6
J

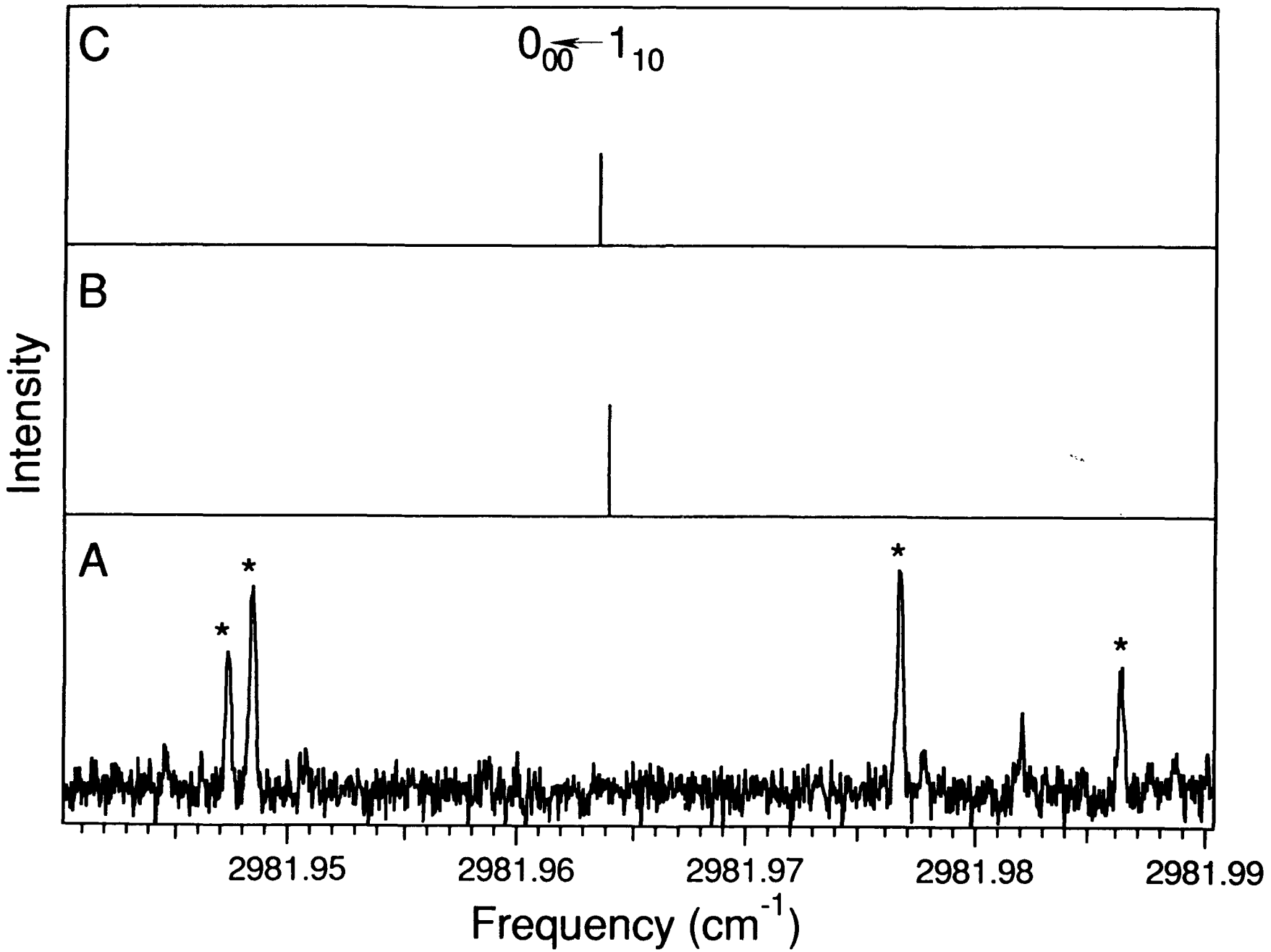
C
$0_{00} \leftarrow 1_{10}$
B
A
Intensity
*
*
*
*
2981.95
2981.96
2981.97
2981.98
2981.99
Frequency (cm^{-1})

TABLE 1:

Freq	I	$J'_{Ka',Kc'}$	$J''_{Ka'',Kc''}$
2985.5710	1.4	$5_{2,4}$	$4_{1,4}$
2985.5646	1.1		
2985.5612	0.9		
2985.5601	0.6		
2985.1919	1.1	$4_{2,3}$	$3_{1,3}$
2985.1784	1.4		
2985.1712	1.3		
2984.7349	2.3	$3_{2,1}$	$2_{1,1}$
2984.7320	1.6		
2984.7279	3.0		
2984.7149	1.4		
2984.5141	1.2	$4_{1,3}$	$3_{0,3}$
2984.5000	2.1		
2984.4304	2.4	$2_{2,0}$	$1_{1,0}$
2984.4288	1.8		
2984.4270	1.5		
2984.4218	2.2		
2984.1155	3.9	$3_{1,2}$	$2_{0,2}$
2984.1104	2.3		
2984.1058	4.4		
2984.0979	1.6		
2983.8738	1.4	$3_{2,1}$	$3_{1,3}$
2983.8710	0.9		
2983.8670	1.6		
2983.8548	0.7		
2983.8263	1.3	$2_{2,0}$	$2_{1,2}$
2983.8248	1.5		
2983.8231	0.8		
2983.8178	1.2		
2983.7450	4.9	$2_{1,1}$	$1_{0,1}$
2983.7443	4.8		
2983.7354	3.2		
2983.6349	1.0	$4_{2,3}$	$4_{1,3}$
2983.6211	1.3		
2983.6138	1.1		
2983.5543	0.8	$5_{2,4}$	$5_{1,4}$
2983.5479	0.9		
2983.5444	0.6		
2983.5433	0.6		
2983.5179	2.4	$4_{0,4}$	$3_{1,2}$
2983.5127	1.4		
2983.5100	0.4		
2983.5086	1.1		
2983.3910	3.2	$1_{1,0}$	$0_{0,0}$
2983.3841	3.6		
2983.3807	2.6		
2983.2577	1.7	$3_{0,3}$	$2_{1,1}$
2983.2551	0.9		
2983.2395	0.7		
2983.2390	1.0		
2983.2334	1.2		
2983.0331	4.1	$1_{1,1}$	$1_{0,1}$
2983.0287	4.2		
2983.0239	1.5		
2983.0194	2.3		

Freq	I	$J'_{Ka',Kc'}$	$J''_{Ka'',Kc''}$
2983.0105	3.6	$2_{1,2}$	$2_{0,2}$
2982.9945	10.0		
2982.9628	3.0	$3_{1,3}$	$3_{0,3}$
2982.9507	3.7		
2982.9466	6.3		
2982.9420	2.4		
2982.9140	2.5	$4_{1,4}$	$4_{0,4}$
2982.9103	4.0		
2982.9051	1.1		
2982.9017	1.7		
2982.4306	4.9	$4_{0,4}$	$4_{1,4}$
2982.4256	4.8		
2982.4230	1.5		
2982.4216	3.7		
2982.3984	1.2	$1_{1,0}$	$2_{0,2}$
2982.3913	1.6		
2982.3877	0.9		
2982.3964	4.3	$3_{0,3}$	$3_{1,3}$
2982.3939	3.0		
2982.3786	1.6		
2982.3781	3.0		
2982.3726	2.0		
2982.3558	3.2	$2_{0,2}$	$2_{1,2}$
2982.3539	1.4		
2982.3531	5.6		
2982.3473	3.9		
2982.3384	2.4		
2982.3289	4.0	$1_{0,1}$	$1_{1,1}$
2982.3254	5.4		
2982.3221	1.0		
2982.0958	1.3	$2_{1,1}$	$3_{0,3}$
2982.0950	1.2		
2982.0864	0.7		
2981.8199	1.0	$3_{1,2}$	$4_{0,4}$
2981.8146	0.7		
2981.8101	1.5		
2981.8014	1.0		
2981.7249	1.1	$4_{1,3}$	$4_{2,3}$
2981.7110	1.2		
2981.6633	1.2	$3_{1,2}$	$3_{2,2}$
2981.6579	0.8		
2981.6533	1.8		
2981.6442	0.5		
2981.6260	0.8	$2_{1,1}$	$2_{2,1}$
2981.6253	0.9		
2981.6169	0.7		
2981.6071	2.4	$1_{0,1}$	$2_{1,1}$
2981.6034	3.0		
2981.6001	1.1		
2981.5510	0.6	$2_{1,2}$	$2_{2,0}$
2981.5347	2.2		
2981.4891	0.5.	$3_{1,3}$	$3_{2,1}$
2981.4779	0.6		
2981.4740	1.2		
2981.4695	0.6		

Freq	I	$J'_{Ka',Kc'}$	$J''_{Ka'',Kc''}$
2981.4072	0.7	$4_{1,4}$	$4_{2,2}$
2981.4034	0.8		
2981.3982	0.6		
2981.3949	0.3		
2981.2300	1.5	$2_{0,2}$	$3_{1,2}$
2981.2283	0.6		
2981.2273	2.7		
2981.2214	2.2		
2981.2125	1.2		
2980.9396	1.4	$1_{1,0}$	$2_{2,0}$
2980.9324	2.1		
2980.9290	1.3		
2980.9151	1.3	$1_{1,1}$	$2_{2,1}$
2980.9104	1.7		
2980.9051	0.7		
2980.9003	1.1		
2980.8394	1.4	$3_{0,3}$	$4_{1,3}$
2980.8369	0.9		
2980.8213	0.7		
2980.8207	1.0		
2980.8151	1.5		
2980.6231	1.8	$2_{1,1}$	$3_{2,1}$
2980.6224	2.0		
2980.6135	1.5		
2980.5586	1.4		
2980.5425	4.4		
2980.4144	2.6	$4_{0,4}$	$5_{1,4}$
2980.4090	1.1		
2980.4064	0.7		
2980.4048	1.0		
2980.3126	1.6	$3_{1,2}$	$4_{2,2}$
2980.3070	1.2		
2980.3022	1.7		
2980.2940	0.7		
2980.1737	0.7	$3_{1,3}$	$4_{2,3}$
2980.1623	0.8		
2980.1580	2.6		
2980.1532	1.2		
2980.0112	0.9	$4_{1,3}$	$5_{2,3}$
2979.9974	0.9		
2979.8755	1.3	$2_{2,0}$	$3_{3,0}$
2979.8738	1.9		
2979.8722	1.2		
2979.8668	0.9		

TABLE 2

$J_{Ka,Kc}$	Δν	<L|H'|D>
$1_{0,1}$	-0.0040	0.00139
	0.0012	0.00187
$1_{1,0}$	-0.0036	0.00194
	0.0032	0.00368
$1_{1,1}$	-0.0066	0.00331
	-0.0022	0.00305
	0.0041	0.00266
$2_{0,2}$	-0.0099	0.00442
	-0.0008	0.00330
	0.0037	0.00059
	0.0050	0.00134
$2_{1,1}$	-0.0042	0.00400
	0.0025	0.00043
$2_{2,0}$	-0.0039	0.00282
	0.0004	0.00110
	0.0024	0.00100
$3_{0,3}$	-0.0109	0.00354
	-0.0069	0.00047
	0.0012	0.00920
	0.0098	0.00183

$J_{Ka,Kc}$	Δν	<L|H'|D>
$3_{1,2}$	-0.0092	0.00394
	0.0003	0.00298
	0.0052	0.00350
$3_{1,3}$	-0.0061	0.00236
	0.0003	0.00225
	0.0104	0.00566
$3_{2,1}$	-0.0108	0.00564
	0.0016	0.00264
	0.0048	0.00199
$4_{0,4}$	-0.0043	0.00129
	-0.0028	0.00193
	0.0015	0.00301
$4_{1,4}$	-0.0062	0.00225
	-0.0022	0.00296
	0.0037	0.00215
$4_{2,3}$	-0.0056	0.00419
	0.0084	0.00722
$5_{2,4}$	-0.0047	0.00082
	-0.0024	0.00226
	0.0033	0.00364

TABLE 3

$J'_{Ka',Kc'}$	$J''_{Ka'',Kc''}$	OBSERVED	DEV
$5_{2,4}$	$4_{1,4}$	2985.5654	0.0009
$4_{2,3}$	$3_{1,3}$	2985.1799	0.0006
$3_{2,1}$	$2_{1,1}$	2984.7284	0.0014
$4_{1,3}$	$3_{0,3}$	2984.5052	0.0031
$2_{2,0}$	$1_{1,0}$	2984.4270	0.0023
$3_{1,2}$	$2_{0,2}$	2984.1087	0.0059
$3_{2,1}$	$3_{1,3}$	2983.8679	0.0009
$2_{2,0}$	$2_{1,2}$	2983.8232	0.0027
$2_{1,1}$	$1_{0,1}$	2983.7423	0.0008
$4_{2,3}$	$4_{1,3}$	2983.6227	0.0001
$5_{2,4}$	$5_{1,4}$	2983.5482	0.0002
$4_{0,4}$	$3_{1,2}$	2983.5139	0.0018
$1_{1,0}$	$0_{0,0}$	2983.3855	0.0001
$3_{0,3}$	$2_{1,1}$	2983.2464	0.0017
$1_{1,1}$	$1_{0,1}$	2983.0278	0.0024
$2_{1,2}$	$2_{0,2}$	2982.9987	0.0026
$3_{1,3}$	$3_{0,3}$	2982.9500	0.0057
$4_{1,4}$	$4_{0,4}$	2982.9091	0.0010
$4_{0,4}$	$4_{1,4}$	2982.4260	0.0012
$1_{1,0}$	$2_{0,2}$	2982.3927	0.0000
$3_{0,3}$	$3_{1,3}$	2982.3864	0.0027
$2_{0,2}$	$2_{1,2}$	2982.3502	0.0015

$J'_{Ka',Kc'}$	$J''_{Ka'',Kc''}$	OBSERVED	DEV
$1_{0,1}$	$1_{1,1}$	2982.3264	0.0031
$2_{1,1}$	$3_{0,3}$	2982.0933	0.0011
$3_{1,2}$	$4_{0,4}$	2981.8112	0.0073
$4_{1,3}$	$4_{2,3}$	2981.7176	0.0047
$3_{1,2}$	$3_{2,2}$	2981.6560	0.0068
$2_{1,1}$	$2_{2,1}$	2981.6229	0.0017
$1_{0,1}$	$2_{1,1}$	2981.6042	0.0028
$2_{1,2}$	$2_{2,0}$	2981.5381	0.0010
$3_{1,3}$	$3_{2,1}$	2981.4766	0.0059
$4_{1,4}$	$4_{2,2}$	2981.4020	0.0007
$2_{0,2}$	$3_{1,2}$	2981.2241	0.0013
$1_{1,0}$	$2_{2,0}$	2980.9336	0.0000
$1_{1,1}$	$2_{2,1}$	2980.9086	0.0018
$3_{0,3}$	$4_{1,3}$	2980.8267	0.0007
$2_{1,1}$	$3_{2,1}$	2980.6201	0.0010
$2_{1,2}$	$3_{2,2}$	2980.5465	0.0022
$4_{0,4}$	$5_{1,4}$	2980.4104	0.0022
$3_{1,2}$	$4_{2,2}$	2980.3055	0.0063
$3_{1,3}$	$4_{2,3}$	2980.1598	0.0069
$4_{1,3}$	$5_{2,3}$	2980.0041	0.0049
$2_{2,0}$	$3_{3,0}$	2979.8727	0.0030

RMS DEVIATION OF 43 I.R MEASUREMENTS = 0.00320 cm^{-1}

TABLE 4:

Fit Parameters:

A"= 0.529638(44)	A'= 0.53223(37)
B"= 0.180479(22)	B'= 0.17944(14)
C"= 0.151046(31)	C'= 0.15087(13)

Center Frequency = 2982.67373(98)